Emergence of Connectivity Motifs in Networks of Model Neurons with Short- and Long-term Plastic Synapses

Eleni Vasilaki^{1,2}, Michele Giugliano^{1,2,3,*},

1 Dept. Computer Science, University of Sheffield, S1 4DP Sheffield, UK.

2 Theoretical Neurobiology and Neuroengineering Laboratory, Dept. Biomedical Sciences, University of Antwerp, B-2610 Wilrijk, Belgium.

3 Laboratory of Neural Microcircuitry, Brain Mind Institute, EPFL, CH-1015 Lausanne, Switzerland.

E-mail: * michele.giugliano@ua.ac.be

Abstract

Recent evidence in rodent cerebral cortex and olfactory bulb suggests that short-term dynamics of excitatory synaptic transmission is correlated to the occurrence of stereotypical connectivity motifs. In particular, it was observed that neurons with short-term facilitating synapses form predominantly reciprocal pairwise connections, while neurons with short-term depressing synapses form unidirectional pairwise connections. The cause of these structural differences in excitatory synaptic microcircuits is unknown.

We propose that these connectivity motifs emerge from the interactions between short-term synaptic dynamics (SD) and long-term spike-timing dependent plasticity (STDP). While the impact of STDP on SD was shown in simultaneous neuronal pair recordings *in vitro*, the mutual interactions between STDP and SD in large networks is still the subject of intense research. Our approach combines a SD phenomenological model with a STDP model that captures faithfully long-term plasticity dependence on both spike times and frequency. As a proof of concept, we explore *in silico* the impact of SD-STDP in recurrent networks of spiking neurons with random initial connection efficacies and where synapses are either all short-term facilitating or all depressing. For identical background inputs, and as a direct consequence of internally generated activity, we find that networks with depressing synapses evolve unidirectional connectivity motifs, while networks with facilitating synapses evolve reciprocal connectivity motifs. The same results hold for heterogeneous networks including both facilitating and depressing synapses. Our study highlights the conditions under which SD-STDP explains the correlation between facilitation and reciprocal connectivity motifs, as well as between depression and unidirectional motifs. These conditions may lead to the design of experiments for the validation of the proposed mechanism.

Author Summary

Understanding the brain requires unveiling its synaptic wiring diagram, which encodes memories and experiences. Synapses are, however, more than mere plugs connecting neurons; they are communication channels implemented by biophysical systems that display history-dependent properties. During prolonged repeated activation, synapses may *functionally* undergo "fatigue" or may "warm up". These effects, known as short-term plasticity, alter temporarily the communication properties of a synapse, i.e., over tens to hundreds of milliseconds. At the same time, synapses undergo *structural* changes that persist from hours to days, known as long-term plasticity.

Recent progress in electrophysiology enabled simultaneous access to the synaptic wiring diagram in microcircuits, and to its short-term features, i.e., the "fatigue" or "warm-up" properties. Non-random connectivity patterns were reported, as i) co-occurrence of "fatigue" features and unidirectional connections between two neurons, or ii) co-occurrence of "warm-up" features and reciprocal connections. We present a biologically plausible explanation for those patterns, based on the interaction of short- and long-term synaptic plasticity. We further formulate a computational model and provide an interpretation of the simulation results by means of its statistical description.

Introduction

Among the most exciting challenges in Neuroscience, the investigation of the brain wiring diagram known as *connectomics* made spectacular progresses and generated excitement for its perspectives (1). Novel discoveries in molecular biology (2; 3; 4), neuroanatomical methods, (5; 6), electrophysiology (7; 8; 9), and imaging (10; 11; 12) have pushed forward the technological limits, for an ultimate access to neuronal connectivity. This is in fact the most important level of organization of the brain (13), pivotal to understanding the richness of its high-level cognitive, computational, and adaptive properties, as well as its dysfunctions.

At the microcircuit level (14; 15; 16; 17; 18), the non-random features of cortical connectivity have recently raised a lot of interest (7; 9). The occurrence of stereotypical connectivity motifs was experimentally demonstrated and, in some cases, accompanied by physiological information on neuronal and synaptic properties (7; 19; 20; 9), on activity-dependent short-term (21; 22) and long-term plasticity (23; 24) and rewiring (25; 26). These physiological details are complementary to anatomical connectivity mapping, and are known to underlie structural, dynamical, and computational network properties (27). In fact, information transmission between neurons in the brain takes place by means of more than mere "connectors". For instance, short-term dynamics (SD) of synaptic efficacy is very common and has been quantified as transient and reversible facilitation or depression of postsynaptic responses, upon repeated presynaptic activation (28). Relaying information to downstream neurons in a microcircuit is thus dependent on past-history, determined by presynaptic activation frequencies, and shaped by the SD profile at each synapse (21).

We address recent experimental findings obtained in rodent cortices (19), where short-term facilitation and depression were found to correlate to specific, pairwise, connectivity motifs: neurons, connected by synapses exhibiting short-term facilitation, form predominantly reciprocal motifs; neurons, connected by synapses exhibiting short-term depression, form unidirectional motifs. Interestingly, the same over expression of connectivity motifs has been observed in another brain area, i.e. the excitatory microcircuitry of the olfactory bulb (29). The cause of these structural differences are largely unknown.

Inspired by the theory by Clopath *et al.* (2010) on the relationship between neural code and cortical connectivity (30), we hypothesise that interactions between short-term and long-term synaptic plasticity could explain the observed pairwise connectivity motifs. In (30), spike-timing dependent long-term synaptic plasticity (STDP) was shown to account *in silico* for the emergence of non-random connectivity motifs in networks of model neurons (30). Adopting the same framework, we add to it a standard phenomenological description of SD (31), and study SD-STDP interactions in recurrent networks of Integrate-and-Fire neurons (32).

Extensive computer simulations of the evolution of synaptic efficacies under both external and self-generated activity have revealed an over-expression of reciprocal motifs on facilitating synapses, and of unidirectional motifs on depressing synapses. The departure from the initial random connection efficacies results from the interplay between neuronal activity and synaptic plasticity mechanisms, over long (STDP) and short time scales (SD). Supported by a mean-field analysis (33; 34; 35; 36; 37), we conclude that the SD-STDP interplay is controlled by the distribution of firing rates in the network, through the switch of STDP from a correlational "pre-post" *temporal* mode at low firing rates, to a "Hebbian" *rate* mode at high firing rates, earlier reported experimentally

by Sjöström *et al.* (38). Short-term facilitation provides a positive feedback in recurrent microcircuits and it boosts firing, while depression acts as a negative feedback and it effectively attenuates high firing rates and discouraging their reverberations. In the "Hebbian" mode, STDP mostly gives rise to long-term potentiation (LTP) of synaptic efficacy, which becomes stronger resulting in reciprocal motifs. This leads to increasing firing rates of bidirectionally coupled neurons, with LTP acting as a long-term positive feedback, until the connection efficacies are ultimately stabilized by saturation. In the "pre-post" (temporal) mode instead, it is the spike timing that drives LTP, which strongly favors the emergence of spatially asymmetric, i.e., unidirectional, motifs (30).

Materials and Methods

We study the properties of networks of excitatory spiking neurons (32), connected via plastic, *current-based*, synapses(21; 31; 36; 35; 30; 37) via a set of simulations. We introduce a convention for distinguishing between "strong" and "weak" connections consistent with (30), and a simple measure to quantify the occurrence of pair-wise motifs in our simulations. We finally provide a Wilson-Cowan firing rate model that is helpful for the interpretation of the numerical results. The numerical values of all parameters are indicated in Table 1.

Neuron model

The network is composed of identical adaptive exponential Integrate-and-Fire neurons (32), each described by a membrane potential $V_m(t)$ and by a spike-frequency adaptation variable x(t)(39). Below a threshold V_{θ} , $V_m(t)$ satisfies the charge-balance equation

$$c_m \dot{V}_m = g_{leak} (E_{leak} - V_m) + g_{leak} \Delta_T e^{(V_m - V_T) / \Delta_T} - x + I_{syn} + I_{ext}$$
 (1)

where I_{syn} is the synaptic input from other neurons and I_{ext} the external (background) input currents. When a spike occurs, i.e., $V_m(t)$ crosses V_{θ} , V_m is reset to a E_{reset} .

The spike-frequency adaptation variable x(t) evolves as

$$\tau_x \dot{x} = a \left(V_m - E_{leak} \right) - x \tag{2}$$

When a spike occurs, x evolves as $x \to x + \Delta_x$. The numerical integration of Eq. 1 is suspended

for a period of time τ_{arp} following each spike, to mimic absolute refractoriness, during which V_m remains "clamped" at E_{reset} .

The model details are not essential to our conclusions (see Supplemental Information, Figure S7).

External (background) inputs

Each neuron is identified by an index i = 1, 2, 3... and it receives a time variant input $I_{ext i}$ according to the following protocols.

Toy Network: (e.g., Fig. 1B, 10 neurons) $I_{ext i}$ consists of a 0.5 nA constant current, as well as periodic 1 nA square pulses. Pulses occur as in a traveling wave of activity, which moves every 5 msec from one unit, e.g., the *i*-th neuron, to its next index neighbour, e.g., the (i + 1)-th neuron, see also (30). Each pulse is delivered in turn to all neuronal indexes, as an extremely narrow bellshaped profile with unitary amplitude and standard-deviation of 0.5, resulting in neighbouring neurons being only slightly stimulated. Each pulse is of sufficient amplitude to elicit neuronal firing in the unit where the bell-shaped profile is centred on, e.g., the *i*-th unit (unless refractory).

Large Network: (e.g., Fig. 5, 1000 neurons) I_{ext} is as in the toy network with the addition of an uncorrelated gaussian noisy current (40), with mean μ , standard deviation $\sigma = 200 \ pA$, and autocorrelation time length $\tau_{syn} = 5 \ msec$. Parameter μ is drawn randomly before launching the simulation and for each neuron of the network, from a gaussian distribution with mean 200 pAand unitary coefficient of variation. The noisy current mimics asynchronous synaptic inputs from (not explicitly modelled) background populations (41; 42).

Internal (synaptic) inputs

Neurons connect to each other according to a fixed anatomical wiring matrix $[C_{ij}]$, which indicates whether neuron *j*-th projects to neuron *i*-th, i.e., $C_{ij} = 1$, or not, i.e., $C_{ij} = 0$. The matrix $[C_{ij}]$ is obtained from an all-to-all connectivity without autapses (i.e., $C_{ii} = 0$), upon randomly pruning $\approx 20\%$ of its elements (see e.g. Fig. 1B), to introduce variability in neuronal firing. A more substantial reduction of the structural connectivity does not affect qualitatively our conclusion, although it downscales the number of plastic synapses available for statistical analysis. This would require larger networks to be simulated in order to obtain the same statistical confidence over our results, and would require upscaling G_{ij} (e.g., through increasing W_{max} , see the next subsections) to obtain the same network firing rates.

The *i*-th neuron receives at any time a synaptic current I_{syn} *i*, described as

$$\dot{I}_{syn\ i} = -I_{syn\ i} / \tau_{syn} + \sum_{j=1}^{N} \sum_{f}^{\infty} C_{ij} G_{ij} \delta(t - t_{j}^{f})$$
(3)

where t_j^f represents the occurrence time of the *f*-th spike emitted by the *j*-th presynaptic neuron, and G_{ij} the amplitude of the postsynaptic current (PSC), corresponding to the activation of the synapse by the presynaptic *j*-th neuron. The Dirac's delta function $\delta(t)$ represents the occurrence of a presynaptic action potential. Eq. 3 models incoming individual PSCs as waveforms with instantaneous rise time and slower decay time (43), imposes a linear postsynaptic superposition of effects, and implies that in the lack of any presynaptic spiking activity, $I_{syn i}$ decays exponentially to zero with a time-constant τ_{syn} , and when a presynaptic spike is fired it evolves as $I_{syn i} \rightarrow I_{syn i} + C_{ij} G_{ij}$.

Frequency-dependent short-term synaptic dynamics (SD)

 G_{ij} defines the amplitude of the PSC from presynaptic neuron *j*-th to postsynaptic neuron *i*-th. On short timescales, its value changes as a function of the activation history of the presynaptic neuron, leading to transient and reversible depression or facilitation of synaptic efficacy (21). This is referred here as homosynaptic plasticity and implemented by having G_{ij} proportional to the amount of used resources for neurotransmission u_{ij} r_{ij} and their maximal availability A_{ij} , i.e., $G_{ij} = A_{ij} u_{ij} r_{ij}$.

Frequency-dependent short-term synaptic dynamics is described by the following equations, with a different set of parameter values to capture depressing or facilitating synapses (21):

$$\begin{cases} \dot{r}_{ij} = (1 - r_{ij})/\tau_{rec} - \sum_{k_j}^{\infty} u_{ij} r_{ij} \delta(t - t_{k_j}) \\ \dot{u}_{ij} = -u_{ij}/\tau_{facil} + \sum_{k_j}^{\infty} U (1 - u_{ij}) \delta(t - t_{k_j}) \end{cases}$$
(4)

For the sake of notation, indexes have been dropped from parameter U as well as from the time constants τ_{rec} and τ_{facil} in Eqs. 4, although in general each synapse has its own parameters (see Table 1). Eqs. 4 reduce to the following update rules: i) when no spike is fired by the presynaptic neuron j, u_{ij} and r_{ij} recover exponentially to their resting values, U and 1, respectively; ii) as a presynaptic spike occurs, r_{ij} is reduced as $r_{ij} \rightarrow (1 - u_{ij}) r_{ij}$, while u_{ij} is increased as $u_{ij} \rightarrow u_{ij} + U_{ij} (1 - u_{ij})$. The impact of short-term plasticity of PSCs amplitude is exemplified in Fig. 1C,F.

Spike-timing dependent long-term plasticity (STDP)

We further extend the description of PSCs (Eqs. 3-4), by an additional scaling factor W_{ij} , to incorporate STDP (24), see also (44):

$$G_{ij} = W_{ij} A_{ij} u_{ij} r_{ij}. ag{5}$$

 W_{ij} changes on timescales longer than τ_{rec} and τ_{facil} and according to the correlated activity of both pre- and postsynaptic neurons, as in (35), capturing spike-triplets effects (35; 30; 37). This is referred here as heterosynaptic plasticity. Each neuron is complemented by four variables, i.e., q_1, q_2, o_1, o_2 , which act as running estimates of the neuron firing rate, averaged over distinct time scales, i.e., $\tau_{q_1}, \tau_{q_2}, \tau_{o_1}, \tau_{o_2}$. In the lack of any firing activity of the *j*-th neuron, those variables exponentially relax to zero:

$$\tau_{q_1} \dot{q}_{1_j} = -q_{1_j} \qquad \tau_{q_2} \dot{q}_{2_j} = -q_{2_j} \qquad \tau_{o_1} \dot{o}_{1_j} = -o_{1_j} \qquad \tau_{o_2} \dot{o}_{2_j} = -o_{2_j} \qquad (6)$$

while each time the neuron fires, these variables are increased by a unit:

$$q_{1_i} \to q_{1_i} + 1 \qquad q_{2_i} \to q_{2_i} + 1 \qquad o_{1_i} \to o_{1_i} + 1 \qquad o_{2_i} \to o_{2_i} + 1. \tag{7}$$

This enables a compact formulation of STDP: when the j-th neuron spikes, the following updates are performed for all the indexes i:

$$\begin{cases} W_{ij} \rightarrow W_{ij} - \eta \ o_{1_i}(t) \left[A_2^- + A_3^- q_{2_j}(t-\epsilon) \right] \\ W_{ji} \rightarrow W_{ji} + \eta \ q_{1_i}(t) \left[A_2^+ + A_3^+ o_{2_j}(t-\epsilon) \right] \end{cases}$$
(8)

as the *j*-th neuron is presynaptic to all connected *i*-th neurons, and postsynaptic to all connected *i*-th neurons, respectively. Numerically, the evaluation of q_{2j} and o_{2j} is performed just before the neuron *j*-th spikes, as indicated by the infinitesimal time-advance notation of ϵ . When no spike occurs, W_{ij} maintains indefinitely its value. The instantaneous value of each W_{ij} is bounded in the range [0; W_{max}]. Unless otherwise stated, W_{ij} is initialized from a uniform random distribution between 0 and W_{max} , prior to the start of each simulation.

We remark that our choice for combining STDP and SD together aims at a phenomenological description of their interactions. It is assumed that all STDP variables are local as well as that STDP and SD models act independently. This allows us to easily analyse network interactions and avoid the paradox of pre-synaptic firing detection under strong short-term depression of synaptic efficacy. In fact, we assume for simplicity that the STDP coincidence-detector is located at each synapse and that such a detector is able to access timing information of presynaptic spikes, regardless on whether they result in large or small PSCs. Similarly, the same coincidence-detector will also sense all the spikes emitted by the post-synaptic neuron. This is the only information required to calculate the long-lasting synaptic modification.

Convention on "strong" and "weak" connections and network symmetry index

In this study, we focus on the appearance or disappearance of a strong connection between two neurons, only for units that are anatomically connected, i.e., $C_{ij} = 1$. For the sake of comparison, we adopted the framework of Clopath *et al.* (2010), where the activity-dependent appearance or disappearance of a connection conventionally occurs in terms of a competition among the "strong" links in a "sea" of weak synapses (7). As in their paper, we adopt the convention of identifying as "strong" those connections whose corresponding STDP synaptic factor W_{ij} is above the 2/3 of its upper bound W_{max} .

With such a definition, we measure the symmetry in the network connectivity by counting reciprocal or unidirectional motifs as (but see e.g., (45) for alternative definitions)

$$s(W) = 1 - (0.5 N (N-1) - M)^{-1} \sum_{i=1}^{N} \sum_{j=i+1}^{N} |W_{ij}^* - W_{ji}^*|$$
(9)

where N is the size of the matrix W, as well as the size of the network. The symmetry index s(W) takes values in the range [0; 1] and depends on the average *similarity* between elements of W that are on symmetric positions with respect to the diagonal. Following our previous convention, W_{ij} and W_{ji} are first normalized and then zero-clipped: $W_{ij}^* = W_{ij} / W_{max}$ if $W_{ij} > 2/3 W_{max}$,

and otherwise $W_{ij}^* = 0$. In Eq. S46, M represents the number of null pairs $\{W_{ij}^*, W_{ji}^*\} = \{0, 0\}$ that occur as a consequence of clipping or by initialization. Evaluating s(W) on networks with a majority of unidirectional connections results in values close to 0 (e.g., Fig. 2A), while its evaluation on networks with a majority of reciprocal connections results in values close to 1 (e.g., Fig. 2B). For uniform random matrices W, the full statistics of s(W) can be calculated (see Supplemental Information) and employed for deriving a significance measure for s as a p-value, representing the probability that the value of s observed in simulations could result by chance. This symmetry measure is useful only *in silico*, where the entire connectivity matrix as well as its maximal synaptic efficacy are known. The same measure cannot be considered as an operational tool for quantifying experimentally-extracted microcircuit connectivity, where statistical counting of connectivity motifs and their comparison to chance-level are relevant (7). Approaching a qualitative comparison to the experiments of Wang *et al.* (2006), such a statistical counting has been used in the large simulations of Fig. 5.

Mean-field Network Description

We approximate the firing rate of the network of Integrate-and-Fire units through its mean-field dynamical description (46; 47; 34), closely following earlier work (31; 36). We consider the simplifying hypotheses that i) the network consists of one or more non overlapping subpopulations of excitatory neurons (see Figs. 4A-B and Fig. 6A) and that ii) neurons within each subpopulation share identical synaptic coupling, connectivity, and short-term synaptic plasticity properties, i.e., all depressing or all facilitating, as in Fig. 6A; see Fig. 7A for an exception. We also assume that iii) for each of the (sub)populations, the individual neuronal firing follows a Poisson distribution, with instantaneous mean firing rate E(h), which depends monotonically on the corresponding overall input currents h. Under these hypotheses, neurons can be only distinguished by the subpopulation they belong to, i.e., depressing D or facilitating F, and their firing can be identified as $E_D(h_D)$ and $E_F(h_F)$. For the case of two subpopulations (Fig. 6A), h_D and h_F evolve over a characteristic time scale τ as

$$\tau \dot{h}_{D} = -h_{D} + J_{DD} E_{D} + J_{DF} E_{F} + \hat{I}_{ext}$$

$$\tau \dot{h}_{F} = -h_{F} + J_{FD} E_{D} + J_{FF} E_{F} + \hat{I}_{ext}$$
(10)

where \hat{I}_{ext} represents the external input, J_{DD} and J_{FF} the average synaptic efficacies of recurrent connections within each subpopulation, and J_{DF} and J_{FD} the average synaptic efficacies of intersubpopulations connections. On a first approximation, J can be considered as the ensemble average of G_{ij} . Firing rates E_D and E_F are computed from h_D and h_F as threshold-linear frequencycurrent response functions: $E_D = [h_D - \theta]_+$ and $E_F = [h_F - \theta]_+$, with $[x]_+ = max\{x; 0\}$ (for alternatives see (48; 49)). J_{DD} , J_{FF} , J_{DF} , J_{FD} undergo plastic changes, on both the short and long time scales: indicating by J_{ab} the coupling between the presynaptic population b and the postsynaptic population a, then $J_{ab} = \hat{W}_{ab} \hat{A}_{ab} \hat{u}_b \hat{x}_b$ with $a, b \in \{D, F\}$. The mean-field variables \hat{u}_b and \hat{x}_b depend only on the presynaptic firing rate E_b , and capture the short-term homosynaptic plasticity in the mean-field approximation of Eqs. 4 (31), as:

$$\begin{cases} \dot{\hat{u}}_D = (U_D - \hat{u}_D) / \tau_{facil D} + U_D (1 - \hat{u}_D) E_D \\ \dot{\hat{x}}_D = (1 - \hat{x}_D) / \tau_{rec D} + \hat{u}_D \hat{x}_D E_D \\ \dot{\hat{u}}_F = (U_F - \hat{u}_F) / \tau_{facil F} + U_F (1 - \hat{u}_D) E_D \\ \dot{\hat{x}}_F = (1 - \hat{x}_F) / \tau_{rec F} + \hat{u}_F \hat{x}_F E_F \end{cases}$$
(11)

On longer timescales, the mean-field approximation of STDP given in (35) is adopted here by altering the factor \hat{W}_{ab} , which evolves as a function of both presynaptic E_b and postsynaptic E_a firing rates:

$$\frac{1}{\eta}\dot{\hat{W}}_{ab} = -A_2^- \tau_{o_1} E_b E_a - A_3^- \tau_{o_1} \tau_{q_2} E_b^2 E_a + A_2^+ \tau_{q_1} E_b E_a + A_3^+ \tau_{q_1} \tau_{o_2} E_b E_a^2.$$
(12)

Results

We hypothesize that synaptic connectivity reflects the interaction of short-term plasticity, such as homosynaptic depression and facilitation (21), with long-term plasticity. Inspired by a recent theory, which links connectivity to spiking activity and to the neural code (30), we ask the question: could known relationships between short-term plasticity and spiking activity in recurrent networks (31; 33; 36) explain the occurrence of connectivity motifs (19; 29) observed experimentally? In support to our hypothesis, we present simulations of networks of excitatory neuron models with activity-dependent plastic connections. We then study the necessary conditions for the emergence of these specific connectivity motifs by standard firing rate models.

A toy microcircuit model

In order to demonstrate and test the key features of our hypothesis, we consider a simplified representation of excitatory neuronal microcircuits, as a network of adaptive exponential Integrateand-Fire units (32). The validity of our results does not depend on the specific details of the model neuron and of its spike-frequency adaptation parameters chosen here (Supplemental Information, Figure S7). Neurons are connected to each other through excitatory synapses (Fig. 1B), whose efficacy undergoes either short- or long-term plasticity. Using a standard model for short-term synaptic dynamics (SD) (21), we simulate homosynaptic, use-dependent modifications of the postsynaptic potentials (PSPs) amplitude. We also employ a recently introduced phenomenological description of heterosynaptic long-lasting potentiation or depression of PSPs, able to capture with great accuracy both spike-timing and frequency effects (35). We refer to this long-term associative plasticity as spike-timing dependent (STDP). Both SD and STDP occur simultaneously with neuronal dynamics, although across distinct timescales. We note that STDP interacts with short-term plasticity as a frequency-independent scaling factor of PSPs amplitude, rather than contributing to a redistribution of synaptic efficacy in the sense of (50; 51) (see Discussion). In addition to excitatory PSPs evoked by trains of presynaptic spikes, neurons receive an external current input, deterministically played back over and over, as a traveling wave of activity (Fig. 1B). Such an external stimulation recreates the temporal coding of Clopath et al. (2010), which imposes deterministic spike-timing correlations among evoked spikes (see Methods). The external input can be regarded an oversimplified generic e.g., thalamic, input with known temporally correlated structure.

We define two microcircuits, identical for all aspects of neuronal properties, maximal synaptic efficacy, anatomical connectivity, and external inputs, with the exception of the SD properties. Specifically, one microcircuit includes exclusively short-term facilitating synapses (Fig. 1C), while the other includes only depressing synapses (Fig. 1F). In order to describe changes in the microcircuit connectivity, we adopt the same framework of Clopath *et al.* (2010) where connections form or disappear via competition among the "strong" links in a "sea" of weak synapses (7) (see Methods). The connectivity, which is randomly initialized, slowly evolves into largely non-random

configurations during the simulation (Fig. 1D,G). At the steady-state, these configurations match the experimentally observed correlations: reciprocal motifs emerge in cell pairs more often than unidirectional motifs, when synapses are facilitating; the opposite occurs when synapses are depressing. This is revealed both by direct inspection of the synaptic efficacy matrix $[W_{ij}]$ (e.g., see Fig. 8) and by quantification of its symmetry index s (see Methods). Although other statistical measures can be defined, as for instance the percentage of weak elements in $[W_{ij}]$ or the sparseness of the emerging connectivity, here we focus on the reciprocal versus unidirectional features of its strong elements, according to the same convention of Clopath *et al.* (2010). When s takes values close to 1, almost all of the existing pairwise anatomical connections are reciprocal and $[W_{ij}]$ is almost a symmetric matrix. On the other hand, for values of s close to 0, unidirectional or very weak connection motifs prevail.

We underline that the prevalence of external inputs over recurrent synaptic inputs (or vice versa) is not imposed a priori but it depends on the interaction between SD and STDP. For facilitating microcircuits, the overall recurrent (synaptic) input that a neuron receives becomes progressively larger than the external input, as soon as more and more reciprocal connectivity motifs are established by STDP. For depressing microcircuits, the opposite holds, as more and more connections are weakened by STDP.

These results, summarized in Fig. 1 for a sample microcircuit composed by ten neurons, have been confirmed over 2000 repeated simulations, analysed in Fig. 2. Over a slow timescale, STDP results in a very small degree of symmetry ($s = 0.01 \pm 0.01$, mean \pm stdev), with high significance ($p < 10^{-4}$) for each of the repeated simulations involving depressing synaptic connections (Fig. 2C). Under identical external inputs to the microcircuit, STDP leads instead to a large degree of symmetry ($s = 0.61 \pm 0.10$, mean \pm stdev), with high significance ($p < 10^{-4}$) in about 75% of the simulations involving facilitating synaptic connections (Fig. 2D). In the remaining 25% of the cases, the resulting symmetry value was in the range [0.25; 0.55], suggesting that to some extent, the variability observed in experiments (19; 29) was replicated in the simulations, where not 100% of the times the motifs correlations emerged. In this simplified example, the variability is attributed mostly to the sparse anatomical connectivity and the irregular firing regimes this imposes. Doubling the simulation time (not shown) led to a very minor reduction of the variability on s, by less than 3% and only for the facilitating synaptic connections, suggesting that stationarity had been already reached.

A simple mechanism for the emergence of motifs

In the microcircuits considered above, the statistics of the anatomical connectivity, the external inputs, as well as the single-neuron properties are identical. Any difference in long-term modification of connections could only arise i) from differences in the collective neuronal activity and take place ii) through the spike-timing and firing-rate dependent mechanisms underlying connection motifs formation, as first described in (30). In the microcircuits considered here, neuronal activity is known to depend on the connectivity and the short-term changes in PSPs amplitude (31). Indeed, during the 2000 simulations of Fig. 2, the microcircuits including short-term depressing synapses collectively fired at $20 \pm 0 Hz$ (see also Fig. 1H), lower than the recurrent microcircuits employing short-term facilitating synapses, which fired at $59 \pm 4 Hz$ (see also Fig. 1E). Facilitating synapses charge up with ongoing presynaptic activity and they recruit more connected neurons, as in a positive feedback. On the contrary, depressing synapses get soon fatigued, resulting into a weaker subsequent recruitment of postsynaptic neurons, whose firing would further depress synaptic efficacy, as in a negative feedback.

We identify such an asymmetry as the cause underlying motifs emergence, and the firing-rate dependence of STDP (24) as its mechanism. In particular, it is the functional switch of STDP from a correlational "pre-post" temporal mode at low firing rates, to a "Hebbian" rate mode at high firing rates, that entirely accounts for the asymmetry in the connectivity motifs. In addition to the spike-timing information (Fig. 2A), the STDP model employed here faithfully captures the strong dependency on the neuronal firing rates (38) (Fig. 2B). For the sake of illustration, we isolate the impact on synaptic efficacy of Eqs. 6,7,8, in a two-neuron system, with one neuron projecting to the other via a single synapse. We simulate the long-term change in PSPs amplitude at that synapse (see Fig. 2B and (35)), imposing 75 pre-post spike pairing events, evoked at different uniform firing frequencies. We study two cases: (i) each presynaptic spike precedes the postsynaptic spike by 10 msec, i.e., $t_{pre} < t_{post}$, or (ii) vice versa, i.e., $t_{pre} > t_{post}$. In agreement with the experiments (38), above 30-40 Hz long-term potentiation (LTP) prevails on long-term depression (LTD), even in those cases when spike-timing per se would promote LTD, i.e., $t_{pre} > t_{post}$. Below that critical frequency, LTP or LTD reflects causal or anti-causal relationships between pre- and post-synaptic firing times, respectively (24).

It follows that facilitating microcircuits would preferentially develop reciprocal connectivity motifs, irrespectively of the spike-timing, due to their higher firing rates that promote LTP. The consequent increased recurrence in the connections would further increase the overall population firing rate, above the *critical* frequency. This increment in the firing rates leads at first place to LTP. Depressing microcircuits instead do not develop preferentially reciprocal motifs, but reflect the asymmetric temporal structure of the input. On a first approximation, their connections would rather not promote persistent high activity regimes; instead they mostly respond to external stimuli. These stimuli are imposed here at low rates and give rise to feed-forward links, due to the repeating traveling-wave features of the stimulation, as in (30).

These specific connectivity and activity configurations are stable when imposing reflecting boundaries, as in the numerical implementation of STDP (52; 51; 53). These boundaries limit the synaptic efficacy to a minimal and a maximal values (see Methods). We also remark that the firing rate dependence of STDP, shown in Fig. 2B, is not captured by all the models proposed in the literature. In our case, the minimal set of STDP model features sufficient for motifs emergence must include the reversal of LTD into LTP at high firing rates.

As a conclusive illustration of the simple mechanism for motifs emergence, we performed additional negative and positive control simulations (Fig. 3), studying the impact of alternative formulations of STDP. By setting $A_3^+ = A_3^- = 0$, and $A_2^+ = 4.5 \ 10^{-3}$ in Eq. 8 and slightly modifying Eq. 7 (see the Supplemental Information) one can reproduce the pair-based STDP model (52; 54). When parameters are adjusted so that this model has an identical spike-timing dependency (i.e., compare Fig. 3A to Fig. 2A), the resulting frequency dependency is completely different (i.e., compare Fig. 3C to Fig. 2B), showing no reversal of LTD into LTP at high frequencies. Vice versa, by inverting signs and swapping the values A_2^+ , A_3^+ , A_2^- , and A_3^- in the same equations, it is possible to ad-hoc reverse the temporal dependency of STDP, as described experimentally for anti-STDP (aSTDP) (55), while leaving the frequency dependence roughly intact (i.e., compare Fig. 3B,D to Fig. 2A,B) and featuring the reversal of LTD into LTP at high frequencies. Of course, this modified "triplet rule" model should not be generalized as novel accurate description of aSTDP, since more data would be anyway needed to access its firing rate dependence. Panels E-H of Fig. 3 repeat the simulations of Fig. 2, and demonstrate that only when the frequencydependence of STDP is realistic (38), the heterogeneity in the network firing rates leads to the emergence of asymmetric connectivity motifs (compare Fig. 3E,G or Fig. 3F,H to Fig. 2C,D).

Large homogeneous microcircuits

Due to the simplicity of the mechanism disclosed above, we can analyse larger populations of neurons interacting via homogeneous and heterogeneous short-term plastic synaptic connections. Prior to running numerical simulations, we qualitatively investigate the generality of our results and the conditions for the asymmetry in the emerging firing rates. We carry out this analysis by a standard Wilson-Cowan firing rate description of neuronal networks dynamics (see Eq. 10) (47). This approach has been already extended to the case of short-term synaptic depression and facilitation (see Eq. 11) (33; 56; 36), long-term Hebbian plasticity (57), or both (58). This technique can be used as long as the characteristic times of long-lasting plasticity are much longer than those of neural and synaptic short-term dynamics, as in our case.

For the sake of simplicity, we initially omit STDP (Eq. 11), and consider recurrent networks of neurons connected by homogeneous synapses, facilitating (Fig. 4A) or depressing (Fig. 4B). We sketch these networks as oriented graphs, where arrows represent connections with average efficacy J_{FF} or J_{DD} , correspondingly. We do not explicitly include inhibition, which, nevertheless, does not qualitatively alter the validity of our results, as examined in the Supplemental Information. Instead, we distinguish whether the average external input to a generic neuron is zero, i.e., referred to as *balanced* inputs ($I_{ext} = 0$ in Eq. 10), or is set to a positive value, i.e., referred to as *unbalanced* inputs, ($I_{ext} = 5$ in Eq. 10). The population firing rates can be studied via standard methods as in dynamical system theory (59), i.e., analyzing the system of Eq. 10 and evaluating their steady-state solutions.

For instance, given a specific combination of external inputs and recurrent average synaptic efficacies, i.e., $J_{FF} = J_{DD} = 4$ for unbalanced inputs and $J_{FF} = J_{DD} = 10$ for balanced inputs, the steady-state solutions of Eq. 10 provides the equilibrium firing rates. These can be then compared to the *critical* frequency of STDP (see Fig. 2B), invoking the same mechanisms for motifs emergence proposed by Clopath *et al.*, (2010): if above the *critical* frequency, then LTP prevails and STDP will reinforce reciprocal synaptic efficacy; if below the *critical* frequency, then LTP or LTD will be determined by spike-timing information. Panels C and D in Fig. 4 illustrate graphically in the plane E, h, the actual location of the steady-state solutions of Eq. 10. These are derived by means of geometrical analysis techniques, similarly to the nullclines intersection methods (59). In fact, at the equilibrium Eq. 10 can be rearranged so that its roots correspond to the intersections between the unitary slope line (dashed) and a given curve (continuous lines; see Supplemental Information). The shape and bending of such a curve depend on the external input I_{ext} and on the SD parameters, so that the firing rates emerging in the recurrent networks of Fig. 4A-B can be compared to each other (33; 56; 36). The dynamical stability of each steady-state solution is displayed by a different marker symbols: circles for stable, squares for unstable equilibrium points. Similarly to Fig. 2B, the approximate location of the STDP *critical* frequency has been indicated by a gray shading. Although we did not chose the parameters of the rate models to quantitatively match the Integrate-and-Fire simulations (40; 57), we conclude that homogeneous facilitating networks generally fire at higher firing rates than depressing networks, for the same set of average synaptic coupling and external inputs, and when engaged in reverberating activity (40).

Mathematically the two networks share the same mean-field description, Eqs. 10-11, although their numerical parameters are considerably different (see Table 1) (19; 29). Specifically, shortterm depressing synapses have a much larger recovery time constant from depression (τ_{rec}) than facilitating synapses. Facilitating synapses have instead a much larger recovery time constant from facilitation (τ_{facil}) than depressing synapses.

Along these lines and by studying the asymptotic limits of the mean-field equations, we found heuristically that the dominating parameter is τ_{rec}^{-1} . This sets an upper limit to the location of any possible firing rate of each network. Then, a network with low values of τ_{rec}^{-1} , i.e., where the time scale of recovery from depression is very long, would fire slower than a network with comparatively higher values of τ_{rec}^{-1} , i.e., where the time scale of recovery from depression is very fast or negligible. These two cases correspond to the depressing and facilitating networks, respectively (Figs. 4A-B).

These general considerations have been validated and confirmed in networks of 1000 neurons, see Methods. In these simulations, neurons are connected with maximal synaptic efficacy A = 6 pA. In order to increase the biological realism, in these large scale simulations we introduce fluctuating random inputs to each neuron, mimicking background network activity (42). Therefore, each neuron receives an uncorrelated noisy current, as well as a periodic wave-like stimuli (see Methods). Figs. 5A-B display the count of the occurrence of unidirectional *versus* reciprocal connectivity motifs. Similar to the small toy model, analysed in Fig. 2, unidirectional depressing connections significantly outnumber the reciprocal depressing connections, while facilitating reciprocal connections prevail on unidirectional facilitating connections. As indicated by Figs. 5D-E, the distributions of the firing rates of the two networks feature the same heterogeneous distributions of firing rates: networks of homogeneous depressing short-term plastic synapses fire at generally low rates, while networks of homogeneous facilitating synapses fire at higher rates. Finally, the symmetry index s, computed after a very long simulation run, results in a value of 0.28 for the depressing network and of 0.99 for the facilitatory network.

Heterogeneous microcircuits

We further study the more general case of a heterogeneous network (Fig. 6A) with two subpopulations: one with facilitating synapses, and the other with depressing synapses. Arrows represent synaptic connections, with average efficacies J_{FF} , J_{DD} , J_{FD} , and J_{DF} . Synapses established within neuronal pairs that belong to the same subpopulation, share, by definition, the same SD properties, i.e., short-term depressing or short-term facilitating, but not both simultaneously. On the contrary, synapses established within neuronal pairs that belong to distinct subpopulations have, by definition, heterogeneous SD properties. Thus a total of five categories of connectivity motifs are possible in this network: facilitatory reciprocal motifs, depressing reciprocal motifs, facilitatory unidirectional motifs, depressing unidirectional motifs, and reciprocal motifs with both facilitation and depression. For the first four categories, experiments support strong non-random occurrences (19; 29). For the case of reciprocal motifs with both facilitation and depression, no extensive experimental information has been published. Our results suggest that non-random occurrences of the first four categories arises from SD-STDP interactions, and predict that the last category should be largely underexpressed, compared to chance level.

We first examine the impact of STDP in a simplified two-neuron system, with one neuron projecting to the other via a single synapse. Figs. 6B,D, show the long-term change in PSPs amplitude as a function of the pre- and postsynaptic firing rates, at that single synapse. Since in a heterogeneous network pre- and postsynaptic firing frequencies may differ, we swept the firing frequencies of the two neurons throughout all the possible combinations, within a realistic range. We study two cases: each presynaptic spike precedes the postsynaptic spike by 10 msec, i.e., $t_{pre} < t_{post}$, or vice versa, i.e., $t_{pre} > t_{post}$. We emphasise that only synapses established within neuronal pairs that belong to distinct subpopulations can experience heterogeneous pre- and postsynaptic firing rates. In this case however, the impact of spike timing information becomes negligible as soon as pre- and postsynaptic neurons fire at different frequencies. In the small minority of cases where this is not true, pre- and postsynaptic frequencies are integer (sub)multiples of each other, and a transient synchronization of spike times occurs periodically. In these circumstances, the timing information has a specific impact, as revealed graphically by bright or dark lines in the plots of Figs. 6B,D. In all other cases, overall plasticity profiles reflect the conventional associative Hebbian LTP/LTD and its consequences (60; 61; 57).

Intuitively, the heterogeneous population of Fig. 6A can lead to the emergence of connectivity motifs. To illustrate this point, we first ignore that subpopulations might interfere with each other's firing rate. We assume that the facilitating and depressing subnetworks would be still characterized by higher or lower firing rates, respectively, as previously presented for homogeneous networks. Then, the LTP/LTD maps of Figs. 6B,D suggest that such an initial asymmetry of emerging firing rates can be maintained indefinitely. The connections J_{DF} are increasingly weakened and the connections J_{FD} strengthen. The resulting configuration, sketched in Fig. 6C, is stable. We tested and confirmed this statement under the mean-field hypothesis, by studying the dynamics of Eqs. 10, 11, and 12, in addition to computing their equilibria. Fig. 6E-F display the mean firing rates of each subnetwork, and the initial time course of synaptic efficacies, with J_{DF} progressively becoming weaker. This is true only when inter-population efficacies, i.e., J_{FD} and J_{DF} , are initialized to slightly weaker values than the intra-population couplings could however emerge from fully homogeneous couplings, i.e., $J_{FF} = J_{DD} = J_{DF} = J_{FD} = 1$, as demonstrated in the Supplemental Information.

We further confirmed that the synaptic configuration, indicated by the mean field models, is present in large microscopic numerical simulations, as in Fig. 5C (see Methods). These simulations involve 1000 identical Integrate-and-Fire units, subdivided in two subpopulations of equal size, with their anatomical connectivity set to 80% of all possible connections, similar to the homogenous case. The maximum synaptic efficacy is set to $A = 12 \ pA$ and the initial synaptic connections W_{ij} are randomly initialized. As in the mean-field model, the inter-population terms W_{ij} are initialized to weaker values than the intra-population terms (but see Supplemental Information for alternatives). Each neuron receives an uncorrelated background noisy current as well as periodic wave-like stimuli, similar to the homogeneous case. As indicated by Fig. 5F, the distributions of the spiking frequencies of individual neurons of the two subnetworks feature the same heterogeneous distribution of firing rates as in the previously studied homogeneous networks: subnetworks of depressing short-term plastic synapses fire at generally low rates, while subnetworks of facilitating synapses fire at higher rates. The location of the *critical* firing frequency for the STDP is represented again as a grey shaded area.

Results in Fig. 5C show all the possible synaptic combinations. As in the data of Wang etal. (2006), reciprocal motifs are significantly co-expressed with facilitatory synapses and unidirectional motifs with depressing synapses. The actual motif count is compared to the null-hypothesis of having statistical independence between the connection occurrence within a pair of neurons, estimated at a 95% confidence interval upon the same hypothesis of *Bernoulli* repeated, independent, elementary events. The frequency Q of observing a connection between two neurons, regardless of its SD properties, is first estimated by direct inspection of the connectivity matrix $[W_{ij}]$. Then the conditional occurrence frequencies of a facilitatory synapse Q_F and of a depressing synapse $Q_D = (1 - Q_F)$ are computed, given that a connection exist between two neurons. The null hypothesis for each possible combination is given by standard probability calculus, under the hypothesis of independence of the identical events. For instance, the occurrence frequency of observing by chance no connections within a neuronal pair is $(1-Q)^2$, while the occurrence of observing by chance a reciprocal motifs with mixed depressing and facilitating properties is $2 (Q^2 Q_F Q_D)$. Finally, in this example, the symmetry index s, computed after a very long simulation run, resulted in a value of 0.18 for the depressing subnetwork and of 0.66 for the facilitation subnetwork.

Microcircuits with overlapping SD properties

In the heterogeneous network of Fig. 6, as well as in the homogeneous networks, we make the assumption that the SD profile is determined primarily by the identity of the projecting neuron. This has been experimentally found in the olfactory, visual, and somatosensory cortices as well as in other brain areas (62; 63; 64; 65). Nonetheless, the assumption on the projection-cell specificity can be removed in order to theoretically explore the impact of SD heterogeneity across distinct synaptic connections established by the same presynaptic neuron (66).

We assumed that a generic neuron had a certain probability p_D of establishing a short-term depressing synapse with a target neuron, and a probability $1 - p_D$ of establishing a short-term facilitating synapse with another one. In this case, individual neurons are still indistinguishable and their mean-field synaptic input can be described mathematically Fig. 7A (see Supplemental Information).

For small values of p_D , the emerging firing rates approximate those of a network of facilitating

synapses, while for large values of p_D the firing rates behave as for a network of depressing synapses. In other words, the mixed networks behave dynamically as an intermediate case between two extremes. This result is quantified in figure Fig. 7B, where the location of the stable equilibrium points has been analysed under the mean-field hypotheses and plotted as a function of p_D , for different external inputs regimes. The qualitative location of the *critical* firing frequency for the STDP is represented as a grey shaded area. In this situation, and as an explicit consequence of the lack of any structure, i.e., compare Fig. 7A with Fig. 6A, STDP fails to discriminate individual connections within the network, but rather shapes them as reciprocal or as unidirectional motifs, depending on the particular choice of p_D .

Discussion

Our results indicate that time- and frequency-dependent STDP mechanisms may be responsible, through internally generated spiking activity in recurrent network architectures, for the observation that excitatory neurons connected by short-term facilitating synapses are more likely to form reciprocal connections, while neurons connected by short-term depressing synapses are more likely to form unidirectional connections. More specifically:

- 1. the internally generated firing rates in model networks with facilitating connections are higher than in networks with depressing connections, under identical background inputs;
- neurons, participating to such an internally generated activity, are likely to form bidirectional connections with each others when firing at sufficiently high rates, reflecting the "Hebbian" mode of STDP; neurons firing at low rates are likely to form unidirectional connections, reflecting the temporally asymmetric "pre-post" temporal mode of STDP;
- 3. once formed, these connectivity motifs persist and self-sustain themselves through the internal firing regimes of the network, from which the motifs emerged from;
- 4. externally generated inputs, strongly depolarizing or strongly hyperpolarizing individual neurons, when prevailing over internally generated activity, may lead to opposite motifs emergence consistent with Clopath *et al.* (2010).

Relationships to previous work and additional mechanisms

The impact of long-term associative synaptic plasticity in recurrent networks of spiking neurons has been earlier studied by many investigators, who proposed mechanisms for the unsupervised formation of stimulus-driven dynamical attractors of network activity, in the context of workingmemory states (57). Within the same aims, the interactions between long-term plasticity and SD were also already partly explored, both in numerical simulations and in mean-field descriptions (58). Here, we focused on specific long-term plasticity mechanisms (STDP) (24) to study the emergence of network structure (67; 68; 69; 70) and connectivity motifs (30; 71). To the best of our knowledge, this is the first time that SD is viewed as key element for the emergence of network connectivity, and shown to capture, to a certain extent, the experimental observations.

Our study builds upon assumptions of Clopath *et al.* (2010): *in silico* activity-dependent (dis)appearance of a connection occurs in terms of a competition among "strong" links in a "sea"

of weak synapses, which are undetectable by cellular electrophysiology. There is still no general agreement on whether STDP and its variants can entirely account for developmental wiring, finetuning, or remapping of microcircuits connections (72). However, the role of STDP for connectivity development has been positively discussed for systems where information is present at fast time scales (73), as it might be relevant for the neural code of cortex and olfactory microcircuitry. In addition, the STDP "triplet" rule proposed by Pfister and Gerstner (35), which is the central ingredient for this work, captures the behaviour of developmental plasticity models (37) widely used in classic studies of connectivity development (74). As a consequence, our results are built upon well-known phenomenological models, which have been shown to have excellent agreement with experimental data sets (21; 35; 30). We have, therefore, neglected more accurate biophysical descriptions of SD (75; 76; 77; 78) and STDP (79; 80), aiming at a minimalist description of neuronal excitability, synaptic transmission, and synaptic plasticity. The advantage of our approach is that the functional consequences of the interactions between SD and STDP could be analysed by standard mean-field analysis (34; 36).

Our study concludes that the symmetry of the connections may be influenced by the internally generated spatio-temporal correlations of neuronal firing (81). Therefore, connectivity motifs might not emerge exclusively from correlations governed by the external inputs (30). Both internally generated and externally imposed correlations are likely to play a role and therefore the results of Clopath *et al.* (2010) still hold. For instance, in a microcircuit connected by purely depressing synapses, external activity can still induce heterogeneity in the firing rates. If a subset of neurons was strongly depolarized by external selective inputs, then units would fire above the critical frequency, and non-random bidirectional connectivity might equally emerge (see Fig. 8). Similarly, strong hyper polarization by external selective inputs, would cause neurons to fire below the critical frequency, even though neurons are connected by recurrent facilitating synapses (not shown)..

Out of many possible features affecting internally generated activity, such as cellular excitability, architecture of long-range connections, and SD properties, here we focused on the last one. We note however that the dataset of Wang *et al.* (2006) contains additional information on cell excitability and its correlation to motif emergence. Cells displaying accommodating discharge patterns (i.e., exhibit spike frequency adaptation) are found to establish mostly unidirectional motifs. Instead, cells displaying nonaccommodating discharge patterns establish mostly reciprocal motifs (19). A differential expression of spike-frequency adaptation currents results in (non)accommodating discharge

patterns. This is known to affect the firing rate distributions in recurrent model networks (82; 83; 39), and generally lower the location of steady-states stable equilibria (Figs. 4C-E). For the model parameters employed here, we did not observe differences when repeating all our simulations without spike-frequency adaptation. Adaptation currents in the model are not strong enough to reduce substantially the steady-state firing rates of e.g., the facilitatory subnetworks below the *critical* firing rate for STDP, and violate our conclusions. On the contrary, as spike-frequency adaptation is reported by Wang *et al.* in neurons participating to unidirectional motifs, we speculate that it participate jointly with depressing SD in maintaining STDP in its correlational "pre-post" mode: once more this determines the emergence of unidirectional connectivity motifs. Non-accommodating discharge patterns would by definition not interfere with the output firing rates, in networks connected by facilitating synapses and bound to emerge reciprocal motifs, by the "Hebbian" mode of STDP.

Our study addresses the emergence of motifs in the cortical pyramidal microcircuitry, but as preliminary data collected in the olfactory bulb become available, our framework could tentatively model a common principle for synaptic wiring. Long-term and short-term plasticity has been experimentally found among olfactory mitral cells, (84; 29), and STDP was reported in the rodent and insect olfactory systems (85; 86), and invoked at the output of mitral cells to explain decorrelation of sensory information (87). We, therefore, speculate that similar mechanisms for the emergence of connectivity motifs are common in both the cortical and olfactory microcircuitry.

Our investigation of heterogeneous network architectures revealed that STDP and SD led to a stable configuration of developing connections, compatible to the experimental observations. Under the simplified hypotheses that we adopted, the configurations of connectivity motifs and their relationship to the underlying neuronal collective dynamics are stable. Our results have been grounded on both numerical simulation results and mean-field analysis. The latter, however, ignored spike-timing correlations between spike-trains. It could thereby only assess the conditions for the emergence of strong connections. While this is sufficient to anticipate the emergence of reciprocal connectivity motifs, its converse does not per se implies the emergence of unidirectional motifs. In such a case, connections would for instance tend to weaken or to disappear. It is only through the numerical simulations of the full network of spiking neurons that we could show that the causal spike-timing information, if present, gives rise to unidirectional connectivity via STDP mechanisms.

We also note that the major difference in SD properties, which accounts for motifs emergence,

is the heterogeneity of the time constant representing the short-term depression recovery τ_{rec} . In this respect, our results and conclusions would be qualitatively unchanged by replacing facilitating synaptic properties with linear, i.e., non-depressing, properties. Along these lines, we hope that our results might prompt new experiments on connectivity motifs. We predict that the value of τ_{rec} , in a pair of connected neurons, should be inversely correlated to the occurrence frequency of reciprocal motifs.

Simplifying assumptions

Among the key simplifying hypotheses of this paper, we note that STDP was assumed to scale only the SD parameter G, while leaving the parameter U unaltered (88). This choice is consistent to what has been reported at distinct synapses of the central nervous system, although it might not be representative of all cortical areas (50). Although the debate on pre- and postsynaptic expression of both SD and STDP is fierce, our choice of SD and STDP interaction is in part an arbitrary hypothesis, and it serves as a first solid ground for our conclusions. Enabling STDP to modify the parameter U would have partly altered in an activity-dependent manner, the SD profile of a synapse. This would have made isolating SD contribution more complex, and relating our findings to previous theoretical works (67; 68; 69; 30; 70) less straightforward.

The model itself is purely phenomenological, and does not capture biophysical details, but rather the interaction of SD and STDP via a set of variables locally known to the synapse. It does however maintains the desirable compatibility with experimental data. In addition, explicit and systematic details on STDP at excitatory facilitatory synapses in the ferret prefrontal cortex are currently scarce (19). While more efforts, both experimental and theoretical, should be undoubtedly devoted in these directions, the hypothesis of scaling G and not U remains a simplifying assumption, in the view of lacking of a systematic understanding on how STDP affects all the parameters of the SD model (89).

The presence of two classes of excitatory cortical synapses (19), with a distinct set of SD parameters such as τ_{rec} , τ_{facil} , and U, prompted us to consider in our model the existence of two classes of excitatory neurons. The consequence of having these classes within the same microcircuitry, as well as their postsynaptic target preferences for connection, are crucial issues that deserve more experimental and theoretical efforts, but see however (36; 90). We thus explicitly neglected heterogeneity in the target synaptic preference of neurons, when expressing a facilitating or depressing SD profile (66). We instead considered homogeneous and heterogeneous neuronal populations, where the facilitating or depressing SD profile was determined by the projecting neuron. Although such a scenario for SD seems realistic for synapses between principal neurons, it might not be accurate for all the synapses in neocortical microcircuits.

The mixed microcircuitry of Fig. 7 and its preliminary analysis are an example of our attempt to relax these assumptions. Depending on the probability of establishing a facilitating (or depressing) connection, fully mixed networks were shown to behave as a continuum between the two extremes of the homogeneous populations studied earlier, i.e., networks of all facilitating or all depressing connections. These mean-field predictions were further confirmed in numerical simulations of large networks (not shown). In these cases, SD-STDP interactions will not necessarily lead to the desirable heterogeneity for the connectivity motifs, as the heterogeneity in the emerging firing rates does not occur. Structured local microcircuit architectures, with heterogeneous single-cell type, number of afferents, and firing rates are the obvious topics for a future study. We believe that the simple case of the heterogeneous two-subpopulation network studied in this work was a first necessary step towards the highlighted future directions.

Another point that deserves some discussion is our choice for a structured, foreground periodic stimulation, employed in all simulations with more or less intense asynchronous background activity. In the toy microcircuit (Fig. 1), the cyclic stimulus was needed to demonstrate the emergence of a large number of asymmetric connections. It is, however, neither a strict requirement for our interpretation of reciprocal and unidirectional motifs formation, nor a necessary condition for their unbalance. This cyclic, deterministic, stimulus is an oversimplified way to invoke the temporal coding strategy of (30). It was chosen to unambiguously relate unidirectional pairwise motifs formation to spiking activity. Without such an input, and under the presence of strong uncorrelated background activity, unidirectional motifs would tend to be very sparse. We underline that our intention was to expose to the very same conditions networks identical in every aspects but in the synaptic SD, and validate the heterogeneity conditions of the connectivity matrix.

Limits of our approach

Our proposed mechanism for non-random pattern emergence is based on the sole interactions between STDP and SD. Obviously, it is unlikely that these mechanisms operate independently of other synaptic phenomena. Homeostatic plasticity could for instance continuously rescale synaptic efficacy and make SD heterogeneities less predominant in determining connectivity motifs. In the lack of *a priori* experimental information, we chose the maximal synaptic efficacy A to share the exact same value for all the microcircuits we examined, in order to ensure a fair comparison. With all its limitations, our proposal may still provide a simple working hypothesis on one component underlying the emergence of connectivity, linked to short-term synaptic dynamics, along the same lines of the theory proposed by Clopath *et al.* (2010). Its validity could be challenged by experiments that interfere and probe the emergent firing activity, e.g., in local *in vitro* cultured microcircuits with known synaptic properties (91). Our framework might be also useful for investigating further structure-function relationships at the subcellular level, by altering the synaptic machinery, or by employing (future) genetically-encoded fluorescent reporters of synaptic efficacy and dynamics. The use of optogenetics and genetically encoded neuronal voltage- and calciumsensors, may lead to experimental validation or falsification of our hypothesis, which might directly contribute to understand short- and long-term plasticity interactions.

Further, the results of our simulations do not automatically capture the over-expression of reciprocal connectivity cortical motifs over the unidirectional ones (7). This is violated in the case of short-term depressing synapses, where the expression of reciprocal motifs is clearly at chance level Fig. 5A, but it is however not the case for Fig. 5B. Clopath *et al.* (2010) model these aspects by employing different neuronal coding strategies, i.e., time- or rate-codes. In our work, in order to isolate the heterogeneity component of SD properties, we considered a common type of spatio-temporal activation and ignored, for the sake of simplicity, heterogeneous neural coding strategies. We are however confident that including more complex network architectures, as well as more specific spatio-temporal correlations, as in Clopath *et al.* (2010), additional non-random features could be explained.

In our results, we use oversimplified network architectures to illustrate that two recurrent excitatory networks, identical in any aspect apart of their synaptic properties, evolve different connectivity motifs. We simulated and studied these models analytically, and we identified the mechanism behind the heterogeneity as frequency-related. It would not be an obvious easy task to explain simultaneously all the properties of cortical connectivity, as experimentally observed (19). The choice of our homogeneous architecture, the lack of cell diversity, and the isolated evolution of neuronal dynamics, considerably differ from the actual cortex as well as from the variety of internal and external stimuli it receives during development and during lifetime. Nevertheless, the choice of our protocol serves in demonstrating a potential mechanisms behind the motif formation, for facilitating and depressing synapses.

We would like to emphasise that our theory refers only to one of many possible, perhaps competing, mechanisms that contribute to stereotypical motifs emergence. Alternative explanations and a causal demonstration of the key ideas we suggest, remain to be provided. It might be of interest exploring to which extent developmental changes in SD, such as the switch from depression into facilitation at synapses between layer 5 pyramidal neocortical neurons (64), occurring after postnatal day (P) 22, are mirrored by changes in motifs statistics. For marginal pair-wise probability of connection, Song *et al.* (2005)(7) report no significant dependence on age, but provide no systematic characterization of motifs statistics beyond P20.

It may be also possible to attempt a chronic manipulation of the firing rates of neuron (sub)populations, by pharmacologically altering synaptic profiles, e.g., modulating postsynaptic receptor desensitisation, changing the presynaptic probability release, or interfering with neurotransmitter recycling. As future directions, more complex heterogeneous anatomical architectures and single-cell properties should be incorporated within the same computational modeling framework. Very specific, non-random initial architectures, e.g., small-world and scale-free (92), could be explored, extending our results towards other aspects that determine reciprocal or unidirectional motifs, possibly beyond the firing levels and towards, e.g., , the density of hub nodes, ranking orders, heavy tails in neighbours distribution, etc.

How critical is the STDP "triplet" rule for the validity of our results? Any STDP model that is able to capture the high frequency effect on plasticity, as revealed by the experiments of Sjöström *et al.* (2001), will reproduce our results if combined with short-term facilitating and depressing synapses. Not all STDP models are consistent with the data of Sjöström . For instance, Froemke and Dan (93) proposed an STDP model capturing pre- and postsynaptic frequency effects. This model predicts that in high frequencies no reversal of LTD into LTP takes place, an inversion that is critical for the mechanism we propose for motifs emergence. Interestingly, however, a generalization of the "triplet" rule that we adopt here is able to capture the experimental data of Froemke and Dan (2002) (94). We also note that pair-based STDP models may still support the emergence of reciprocal connectivity motifs and replicate our results (not shown). In fact, by adjusting the numerical values of its parameters (e.g., $A_2^+ = 2A_2^-$ in Eqs. S39 and S42, see Supplemental Information), LTP can be made prevailing over LTD above a frequency similar to the critical value of the triplet-model (72; 95). Nevertheless, when the pair-based STDP parameters are chosen to match the 10Hz temporal window of the triplet-STDP model employed here (compare Figs. 2A and 3A), the frequency-dependent profile observed by Sjöström *et al.* (2001) is not reproduced (compare Figs. 2B and 3C) and SD-STDP interactions do not lead to the same results (compare Figs. 2C,D and 3E,G). This served here as a negative controlsk for our results. We also remark that excluding heterogeneity in spike propagation delays made our analysis simpler. It is known that the distribution of delays considerably affect emerging network states, besides having an obvious effect on STDP (96). In this respect, not only STDP and SD interactions might be altered by propagation delays, but the collective dynamical properties of recurrent networks could also vary. Once more, for the sake of simplicity we chose to consider a minimalist scenario, setting the ground for future, more extended, investigations.

Finally, we underline the great value of the availability of physiological information accompanying anatomical connectivity. These complementary data-set contains precious statistical information regarding the expression of microcircuit motifs, which we are starting to recognize (7; 9). We believe that computational modeling is in this context a very powerful tool to explore additional hypotheses and challenge further theories.

Acknowledgments

We are grateful to C. Clopath, J.-P. Pfister, M. Pignatelli, A. Carleton, P. Dayan, A. Loebel for discussions and comments.

A Supplementary Text

For the sake of illustration of the standard mathematical techniques employed in the main text, we consider two extreme simplifications of the mean-field description of a recurrent networks with short-term plastic synapses (Eqs. 9-10; see also (36), and references therein): the predominance of depressing mechanisms or the predominance of facilitatory mechanisms. We analyze these two cases and specifically study the stability of dynamical equilibria. These simplified models and their analysis have been already provided in the literature, with varying degree of details. We further comment on the analysis of the full model of short-term synaptic plasticity and comment on the impact of adding recurrent inhibition to our scenario. We then consider and numerically analyse the mean-field description of a mixed population, where a generic neuron may establish simultaneously depressing and facilitating synapses to its targets. We finally examine and partly relax the necessary conditions for a heterogeneous network of two interacting subpopulations to display emergence of connectivity motifs. For the case of a random matrix (i.e., as a null hypothesis), we provide some of the statistical properties of the symmetry measure we adopted to quantify the connectivity motifs to derive a confidence measure. In the last section, we provide model details for the pair-based, STDP as well as for the anti-STDP "triplet" model, discussed in the main text.

A.1 A single population with depressing synapses

1

The Eqs. 9-10 of the main text can be simplified under the hypothesis of very fast recovery from facilitation. This is the same of assuming that τ_{facil} is very small and that u = U does not vary in time, as a consequence. In this case, only short-term depression is modifying the synaptic efficacy, so that the mean-field firing rate dynamics of a large recurrent network of excitatory neurons, can be described by a system of two dynamical equations (33):

$$\begin{cases} \tau \dot{h} = -h + A U x E + I_{ext} \\ \dot{x} = (1 - x) / \tau_{rec} - U x E \end{cases}$$
(S13)

These are coupled non-linear differential equations that can be analyzed by standard methods of dynamical systems theory (59). We will consider here the derivation of the equilibria for h and x, and indicate how their stability was assessed. By definition of equilibrium, $\dot{h} = 0$ and $\dot{x} = 0$ for those points (also called *fixed* points). Substituting these conditions in Eqs. S13, we obtain two non-linear algebraic equations,

$$\begin{cases}
h = A U x E + I_{ext} \\
x = 1 / (1 + U \tau_{rec} E)
\end{cases}$$
(S14)

Using the second equation to replace x as it appears in the first, we get an implicit equation in the unknown h:

Connectivity Motifs by Synaptic Plasticity

$$h = A U E / (1 + U \tau_{rec} E) + I_{ext}$$
(S15)

Eq. S15 can be solved numerically (e.g., by the Newton-Raphson method, (97)), given a specific set of parameters A, U, τ_{rec} , and I_{ext} . Alternatively, its solution(s) can be interpreted graphically as the intersection(s) between two functions of h, $F_1(h)$ and $F_2(h)$, in the cartesian plane,

$$\begin{cases}
F_1(h) = h \\
F_2(h) = A U E / (1 + U \tau_{rec} E) + I_{ext}
\end{cases}$$
(S16)

with $F_1(h)$ is the unitary slope line (see Fig. S1). Retaining the graphical interpretation, it is possible to appreciate intuitively the existence of the equilibrium points and their dependence on the parameters, as explored in Fig. S1. To this aim it is useful, prior to plotting $F_2(h)$, to analytically determine some of its mathematical properties, such as the asymptotic limits and derivatives.

We observe that, by definition of $E = [\alpha (h - \theta)]_+$, $F_2(h)$ is zero for values of h lower than θ , $h \leq \theta$. As $h \to +\infty$, $F_2(h)$ tends to an horizontal positive asymptote, occurring at $(J \tau_{rec}^{-1} + I_{ext})$. For values of h larger than θ , the first derivative of $F_2(h)$ is always positive, indicating that the function is monotonically increasing. In the same range of h, the second derivative is instead always negative, therefore indicating that the function is convex. Moreover, the tangent line to $F_2(h)$ at $h = \theta$ is the steepest of all the tangents to subsequent points $(h > \theta)$.

$$\begin{cases} \dot{F}_{2}(h) = \alpha A U / [1 + \alpha \tau_{rec} U (h - \theta)]^{2} \\ \ddot{F}_{2}(h) = -2 \alpha^{2} \tau_{rec} A U^{2} / [1 + \alpha \tau_{rec} U (h - \theta)]^{3} \end{cases}$$
(S17)

The value of the slope of the tangent line at $F_2(h)$ at $h = \theta$ is particularly informative when drawing $F_2(h)$, since at any coordinates $h > \theta$ all the other tangent lines are by definition less steep than it. This maximal slope $(\dot{F}_2(\theta) = \alpha A U)$ can then be used as a necessary condition for the intersections between $F_2(h)$ and the unitary slope line, at least when $I_{ext} \leq \theta$.

When $I_{ext} \leq 0$, there is always an intersection between $F_2(h)$ and $F_1(h)$ at $h = I_{ext}$. This

is a stable equilibrium point (i.e., see below for the discussion of the stability). If $\alpha A U \leq 1$, there will be for $I_{ext} \leq 0$ no other intersections, since $F_1(h) = h$ has unitary slope itself. Given the necessary condition $\alpha A U > 1$, there exist a minimal value for those parameters, above which other two intersections (i.e., one stable and one unstable) with the unitary slope lines occur (compare Fig. S1A,B, and C, which were obtained for increasing values of A).

Determining analytically such values requires imposing the condition where the unitary slope line becomes tangent to $F_2(h)$. Mathematically this can be expressed by stating that when $I_{ext} \leq \theta$ there is a specific (intersection) point $h_0 > \theta$ between $F_1(h)$ and $F_2(h)$. By definition, this point lays on the unitary slope line $F_2(h_0) = h_0$, with $\dot{F}_2(h_0) = 1$, i.e., $F_2(h)$ has a unitary first derivative at h_0 (see Fig. S1B).

$$\begin{cases}
F_2(h_0) = \alpha A U (h_0 - \theta) / (1 + \alpha \tau_{rec} U (h_0 - \theta)) + I_{ext} = h_0 \\
\dot{F}_2(h_0) = \alpha A U / [1 + \alpha \tau_{rec} U (h_0 - \theta)]^2 = 1
\end{cases}$$
(S18)

Simplifying the algebraic manipulations, we note the apparent similarities between the two equations above. We express (part of the) numerator and denominator of the right hand sides of each equations, by denoting the common terms as N_0 and D_0 , respectively, as it follows

$$\begin{cases}
F_2(h_0) = N_0 (h_0 - \theta) / D_0 + I_{ext} = h_0 \\
\dot{F}_2(h_0) = N_0 / D_0^2 = 1
\end{cases}$$
(S19)

Thus, from the second equation we derive $N_0 / D_0 = D_0$, and we substitute it in the first, obtaining

$$h_0 = \theta + \sqrt{(\theta - I_{ext}) / (\alpha U \tau_{rec})}$$
(S20)

The above expression is of course only defined when the argument of the square root is positive, which is consistent with our previous hypothesis (i.e., $I_{ext} < \theta$). One can now replace h_0 in the second equation of Eqs. S19 and obtain the corresponding critical value of A, associated to the existence of such a (double) intersection (Fig. S1B): Connectivity Motifs by Synaptic Plasticity

$$A_0 = \left(1 + \sqrt{\alpha \ U \ \tau_{rec} \ (\theta - I_{ext})}\right)^2 / \ (\alpha \ U) \tag{S21}$$

In summary, when $I_{ext} \leq \theta$ there is always one (stable) equilibrium at $h = I_{ext}$ and of possibly other two intersections (one stable and one unstable; compare Fig. S1A,B, and C), depending on the strength of A with respect to A_0 . For $I_{ext} > \theta$, the situations changes and the scenario simplifies considerably, with only one (stable) intersection for any other choice of the parameters (see Fig. S1D).

The analysis of the stability of the equilibrium points conclude our discussion. Since the dynamical system described Eqs. S13 is non-linear, stability of equilibrium points must be related to the linearized system. The linearization is obtained for each equilibrium point by first-order Taylor expansion of Eqs. S13 around that point. Let's compactly rewrite Eqs. S13 as

$$\begin{cases} \dot{h} = G_1(h, x) = (-h + A U x E + I_{ext}) / \tau \\ \dot{x} = G_2(h, x) = (1 - x) / \tau_{rec} + U x E \end{cases}$$
(S22)

The linearized system, around a generic equilibrium point (h_0, x_0) , is then

$$\begin{cases} \dot{h} \approx G_1(h_0, x_0) + \partial G_1 / \partial h|_{(h_0, x_0)} (h - h_0) + \partial G_1 / \partial x|_{(h_0, x_0)} (x - x_0) \\ \\ \dot{x} \approx G_2(h_0, x_0) + \partial G_2 / \partial h|_{(h_0, x_0)} (h - h_0) + \partial G_2 / \partial x|_{(h_0, x_0)} (x - x_0) \end{cases}$$
(S23)

Assessing the stability of the above system reduces to studying the Jacobian matrix M:

$$M(h_0, x_0) = \begin{pmatrix} \partial G_1 / \partial h & \partial G_1 / \partial x \\ \\ \partial G_2 / \partial h & \partial G_2 / \partial x \end{pmatrix}|_{(h_0, x_0)}$$
(S24)

By definition, it is possible to make explicit the Jacobian matrix as

Connectivity Motifs by Synaptic Plasticity

$$M(h_0, x_0) = \begin{pmatrix} (-1 + \alpha \ A \ U \ x_0) / \tau & (\alpha \ A \ U \ (h_0 \ - \ \theta)) / \tau \\ -\alpha \ U \ x_0 & -\tau_{rec}^{-1} \ - \ \alpha \ U \ (h_0 \ - \ \theta) \end{pmatrix}$$
(S25)

In particular, the real part of the two eigenvalues associated to $M(h_0, x_0)$ has been analyzed for each equilibrium point (h_0, x_0) . The eigenvalues $\lambda_{1,2}$ were computed as the roots of the following algebraic second order equation

$$det\left(I - \lambda M(h_0, x_0)\right) = 0 \tag{S26}$$

where I indicated the 2 × 2 identity matrix and det() indicates the computation of the determinant of a square matrix. When at least one of the eigenvalue had positive real part, the equilibrium point was classified as *unstable*. When both eigenvalues had negative real parts, the equilibrium point was classified as *stable*. Nothing can be however concluded on the stability of the non-linear system, in the cases in which one or both eigenvalues have zero real part (and the other has negative real part). Stable and unstable equilibrium points have been graphically represented as circles and squares in Fig. S1, respectively, as well as in Figure 4C-E.

A.2 A single population with non-depressing facilitating synapses

The Eqs. 9-10 of the main text can be again simplified under the hypothesis of very fast recovery from depression τ_{rec} . The mean-field firing rate dynamics of a single neuronal population, recurrently connected by short-term plastic synapses, can be rewritten as:

$$\begin{cases} \tau \dot{h} = -h + A u E + I_{ext} \\ \dot{u} = (U - u) / \tau_{facil} + U (1 - u) E \end{cases}$$
(S27)

While this hypothesis is not as realistic as the one of the previous section, it is preparatory for the analysis of the full model. As for the previous case, we consider the derivation of the equilibrium points for h and u as well as the assessment of their stability. Substituting the definitions of equilibrium, $\dot{h} = 0$ and $\dot{u} = 0$, into Eqs. S27, we get

$$\begin{cases}
h = A u E + I_{ext} \\
u = U (1 + E \tau_{facil}) / (1 + U \tau_{facil} E)
\end{cases}$$
(S28)

Using the second equation to replace u as it appears in the first, one obtains an implicit equation in h:

$$h = A U (1 + E \tau_{facil}) E / (1 + U \tau_{facil} E) + I_{ext}$$
(S29)

As for Eq. S15, numerical methods can be used for solving Eq. S29, looking for values of h that satisfy the equivalence given a specific set of parameters A, U, τ_{facil} , and I_{ext} . The solution(s) of Eq. S29 can be also graphically interpreted as the intersection(s) in the cartesian plane of two functions of h, $F_1(h)$ and $F_3(h)$ as defined below

$$\begin{cases}
F_1(h) = h \\
F_3(h) = A U (1 + E \tau_{facil}) E / (1 + U \tau_{facil} E) + I_{ext}
\end{cases}$$
(S30)

We observe that by definition of $E = [\alpha (h - \theta)]_+$, $F_3(h)$ is zero when $h \leq \theta$. When $h \rightarrow +\infty$, the function diverges to infinity, but it can also be approximated by the straight line $F_3(h) \approx \alpha A h$. We also note that for values of h larger than θ , the first derivative of $F_3(h)$ is positive, indicating that the function is monotonically increasing. In the same range of h, the second derivative is also positive, therefore indicating that the function is concave.

$$\begin{cases} \dot{F}_{3}(h) = \frac{\alpha \ A \ U \left[1 + 2 \ \alpha \ \tau_{facil} \ (h - \theta) + \alpha^{2} \ \tau_{facil}^{2} \ U \ (h - \theta)^{2}\right]}{[1 + \alpha \ \tau_{facil} \ U \ (h - \theta)]^{2}} \\ \ddot{F}_{3}(h) = 2 \ \alpha^{2} \ \tau_{facil} \ A \ U \ (1 - U) \ / \ [1 + \alpha \ \tau_{facil} \ U \ (h - \theta)]^{3} \end{cases}$$
(S31)

As opposed to the previous case, the value of the slope of the tangent line at $F_3(h)$ at $h = \theta$ is not particularly relevant when drawing $F_3(h)$, since at any coordinates $h > \theta$ all the other tangent lines are by definition steeper than it. The minimal slope is $\dot{F}_3(\theta) = \alpha A U$ can then used in combination with the asymptotic approximation $F_3(h) \approx \alpha A h$ (i.e., the maximal slope is αA). It is then clear that, for $0 \leq I_{ext} \leq \theta$, a sufficient and necessary conditions for having always two equilibrium points (i.e., one stable at the value $h = I_{ext}$ when $0 \leq I_{ext} \leq \theta$, and the other unstable) is represented by $\alpha A > 1$ (Fig. S2A,B). All the considerations on how to assess the dynamical stability of these equilibrium points hold, and the expression of the *Jacobian* matrix M, whose eigenvalues determine the stability, is given below:

$$M(h_0, u_0) = \begin{pmatrix} (-1 + \alpha \ A \ u_0)/\tau & (\alpha \ A \ U \ (h_0 \ - \ \theta))/\tau \\ -\alpha \ U \ (1 \ - \ u_0) & -\tau_{facil}^{-1} \ - \ \alpha \ U \ (h_0 \ - \ \theta) \end{pmatrix}$$
(S32)

A.3 Single population with short-term plastic synapses

In the general case, the mean-field equations of a single neuronal population, recurrently connected by short-term plastic synapses, are given by

$$\begin{cases} \tau \dot{h} = -h + A u x E + I_{ext} \\ \dot{x} = (1 - x) / \tau_{rec} - u x E \\ \dot{u} = (U - u) / \tau_{facil} + U (1 - u) E \end{cases}$$
(S33)

with the neuronal gain function chosen as a threshold-linear relationship between input (mean) current h and output firing rate $E = [\alpha (h - \theta)]_+$ (see also Eqs. 9-10 of the main text). The analysis of this system, including its equilibrium points, has been already given elsewhere (36). Supporting the necessary condition on the symmetry breaking by long-term plasticities mentioned in the Results section of the main text, here we derive a simple observation on the analytical properties of these equilibrium points. According to the definition, we substitute $\dot{h} = 0$, $\dot{x} = 0$, and $\dot{u} = 0$ into Eqs. S33, and get Connectivity Motifs by Synaptic Plasticity

$$\begin{cases}
h = A u x E + I_{ext} \\
x = 1 / (1 + u \tau_{rec} E) \\
u = U (1 + E \tau_{facil}) / (1 + U \tau_{facil} E)
\end{cases}$$
(S34)

By appropriate substitutions of x and of u into the first equation, it is possible to express it as $h = F_4(E(h))$, an implicit equation in h:

$$F_4(E) = \frac{AU\left(E^{-1} + \tau_{facil}\right)}{E^{-2} + E^{-1}U\tau_{facil} + E^{-1}U\tau_{rec} + U\tau_{facil}\tau_{rec}} + I_{ext}.$$
 (S35)

We observe that for $h \to +\infty$, $E(h) \to +\infty$ and $F_4(E) \to A \tau_{rec}^{-1} + I_{ext}$, implying the existence of an horizontal asymptote. This intuitively suggests that for any choice of the other parameters compatible with the existence of multiple equilibrium points (i.e., intersections between $F_4(h)$ and the unitary slope line), the uppermost equilibrium point (i.e., always stable) will change its location proportionally to A and to τ_{rec}^{-1} , for the same choice of I_{ext} . Hence, a high value of τ_{rec} , as in depressing synapses, will give a lower asymptote versus a low value, as in facilitating synapses.

Let's now consider two independent populations of excitatory neurons, one recurrently connected by short-term depressing synapses (i.e., $\tau_{rec} > \tau_{facil}$) and one by short-term facilitating synapses (i.e., $\tau_{facil} > \tau_{rec}$) and both receiving identical non-zero external inputs I_{ext} . As for the previous considerations on the horizontal asymptote of $F_4(E)$, for an appropriate choice of A(i.e., large enough to have multiple equilibrium points) or for any value of $I_{ext} > \theta$, the firing rate uppermost equilibrium point of the facilitating population will always be larger than the firing rate uppermost equilibrium point of the depressing population. Together with the specific firing rate dependence of STDP, arising from the triplet-interactions, this consideration rules out that reciprocal motifs of short-term depressing synapses will outnumber unidirectional motifs of facilitating synapses. The stability analysis for the depressing and facilitating populations (with the parameters used in our simulations) is provided in the main text (see Fig. 3D-F).

Assessing the stability of the above system reduces to linearization of the system around the fixed points by the use of a Taylor expansion and the study of the so called *Jacobian* matrix

 $M(h_0, x_0, u_0)$ of the system, which for the sake of completeness, we report below:

$$\begin{pmatrix} (-1 + \alpha A u_0 x_0)/\tau & (\alpha A u_0 (h_0 - \theta))/\tau & (\alpha A x_0 (h_0 - \theta))/\tau \\ -\alpha u_0 x_0 & -\tau_{rec}^{-1} - \alpha u_0 (h_0 - \theta) & -\alpha x_0 (h_0 - \theta) \\ \alpha U (1 - u_0) & 0 & -\tau_{facil}^{-1} - \alpha U (h_0 - \theta) \end{pmatrix}$$
(S36)

A.4 The impact of recurrent inhibition

We extend the description of the system given in Eqs. S13, to the case where recurrent inhibition is explicitly accounted for. The mean-field firing rate dynamics of two neuronal populations, one excitatory and one inhibitory, recurrently connected by short-term excitatory plastic synapses and by frequency-independent inhibitory synapses (as in Fig. S3), can be rewritten as:

$$\begin{cases} \tau_{e} \dot{h_{e}} = -h_{e} + A_{ee} U x E - A_{ei} I + I_{ext} \\ \tau_{i} \dot{h_{i}} = -h_{i} + A_{ie} U x E \\ \dot{x} = (1 - x) / \tau_{rec} + U x E \end{cases}$$
(S37)

with $E = [\alpha_e (h_e - \theta_e)]_+$ and $I = [\alpha_i (h_i - \theta_i)]_+$. We consider here the derivation of the equilibrium points for h_e , h_i , and x, and we indicate how their stability was assessed. Substituting the conditions $\dot{h_e} = 0$, $\dot{h_i} = 0$, and $\dot{x} = 0$ in Eqs. S37, we obtain three non-linear algebraic equations

$$\begin{cases}
h_e = A_{ee} \ U \ x \ E \ - \ A_{ei} \ I \ + \ I_{ext} \\
h_i = A_{ie} \ U \ x \ E \\
x = 1 \ / \ (1 \ + \ U \ \tau_{rec} \ E)
\end{cases}$$
(S38)

Using the second and third equations to replace x and I in the first, we get an implicit equation in the unknown h_e : Connectivity Motifs by Synaptic Plasticity

$$h_e = \frac{A_{ee} U E}{1 + U \tau_{rec} E} - A_{ei} \left[\alpha_i \left(\frac{A_{ie} U E}{1 + U \tau_{rec} E} - \theta_i \right) \right]_+ + I_{ext}$$
(S39)

We make the assumption that the synaptic coupling from the excitatory to the inhibitory population is sufficiently strong $A_{ie} > \tau_{rec} \theta_i$, so that short-term depression of that pathway does not prevent steady recruitment of inhibition at higher firing rates of the excitatory population. We also assume for simplicity that recurrent excitation is also sufficiently strong so that $A_{ee} > \alpha_i A_{ei} A_{ie}$. Under these hypotheses, when E is below a certain value, i.e., $E < \theta_i / [U (A_{ie} - \tau_{rec} \theta_i)]$, the above implicit equation coincides with Eq. S15 and it can be written as if inhibition was not present:

$$h_e = A_{ee} U E / (1 + U \tau_{rec} E) + I_{ext}$$
(S40)

Instead, above that critical value for E (i.e., and therefore for h_e), Eq. S39 does not change formally, apart from its coefficients:

$$h_e = \hat{A}_{ee} U E / (1 + U \tau_{rec} E) + \hat{I}_{ext}$$
(S41)

with $\hat{A}_{ee} = A_{ee} - \alpha_i A_{ei} A_{ie}$ and $\hat{I}_{ext} = I_{ext} + \alpha_i \theta_i A_{ei}$. It is easy to verify that $0 < \hat{A}_{ee} < A_{ee}$ and $\hat{I}_{ext} > I_{ext}$.

The critical value for the recurrent inhibitory inputs to affect the excitatory population can be translated into a condition on h_e , i.e., $h_e > \theta_e + \theta_i / [\alpha_e U (A_{ie} - \tau_{rec} \theta_i)]$. Under our previous hypothesis, such a critical value for h_e is always larger than the threshold θ_e for the activation of the excitatory neurons. There will exist a range of activation for h_e above θ_e , where the impact of inhibition is negligible. For larger activation h_e , inhibition kicks by step-wise decreasing the parameter \hat{A}_{ee} .

All in all, the presence of recurrent inhibition in the system does not alter qualitatively the conclusions on the existence of equilibrium points of the mean field description. The statement on the separation of the uppermost equilibrium points, associated respectively to the short-term depressing and the short-term facilitating networks, remains true, since the horizontal asymptote shares the same indirect proportionality relationship with the time constant τ_{rec} of recovery from depression.

A.5 Single population with mixed synapses

We consider the special case of a homogeneous network of neurons, whose connections to distinct target postsynaptic neurons can be simultaneously short-term depressing and short-term facilitating. For the sake of simplicity and for distinguishing this case from the mixed populations studied in the main text (see Fig. 4), neurons are assumed to be indistinguishable from each other. However, every neuron has a certain probability p_D to establish a short-term depressing connection with its postsynaptic target. The same neuron has probability $1 - p_D$ to establish a short-term facilitating connection to another postsynaptic neurons. Under these simplifying hypotheses, and by definition of conditional expected value (98), the mean-field firing rate dynamics of the neuronal population, recurrently connected by short-term plastic synapses, is

$$\tau \dot{h} = -h + A \left[p_D u_D x_D + (1 - p_D) u_F x_F \right] E + I_{ext}$$

$$\dot{x_D} = (1 - x_D) / \tau_{rec_D} - u_D x_D E$$

$$\dot{u_D} = (U_D - u_D) / \tau_{facil_D} + U_D (1 - u_D) E$$

$$\dot{x_F} = (1 - x_F) / \tau_{rec_F} - u_F x_F E$$

$$\dot{u_F} = (U_F - u_F) / \tau_{facil_F} + U_F (1 - u_F) E$$

$$(S42)$$

The cases $p_D = 0$ and $p_D = 1$ have been already examined in the previous sections. For intermediate values of p_D , an evaluation of the equilibria of Eqs. S42 has been carried out numerically, resulting in a qualitatively similar behavior to the extreme cases, with the location of the (stable) equilibrium points to be intermediate between those of a short-term depressing neuronal network and those of a short-term facilitation neuronal network. As expected, for increasing values of p_D the location of all equilibrium points of E(h) (if any) decreases monotonically.

A.6 Emergence of motifs when initial intra- and inter-population coupling are identical

A specific initial configuration for the intra- (i.e., J_{FF} , J_{DD}) and inter-population synaptic efficacies (i.e., J_{FD} , J_{DF}) has been indicated in the main text as a necessary condition for subsequent "symmetry-breaking" of the spontaneously emerging firing rates, in the depressing and the facilitating subpopulations (Fig. 4A,C). In this section, we relax such a condition and show how, by an appropriate external stimulation protocol, the same symmetry breaking could occur. As a consequence, the emerge of connectivity motifs is generally not impaired when synaptic couplings are set to identical values (i.e., $J_{FF} = J_{DD} = J_{FD} = J_{DF}$). Other protocols and conditions might lead to the same configuration and here we focus on the simplest.

We assume that the two subpopulations receive a common external input and an alternating pulsed stimulus component. As in a recurring traveling wave of external activity, each subpopulation is alternatively exposed to an pulsating input component, so that both facilitatory and depressing subpopulations are activated but never at same time. Due to intrinsic subpopulation properties, determined by short-term synaptic plasticities and reviewed in the previous sections, and as a direct consequence of the associative character of long-term plasticity (Fig. 4B,D) discussed in the main text, this stimulation protocol leads to stronger intra-population synaptic coupling and weaker inter-population synaptic coupling (see Fig. S5). As discussed in the results of the main text, such a configuration is retained indefinitely, even in the absence of external alternating stimulation.

In order to understand why such a stimulation protocol succeeds in developing inter- and intrapopulation coupling asymmetries, we must examine the STDP parameters (e.g.,) in its mean field formulation (see Eq. 11 of the man text). Let's assume that the firing rate E_D of the depressing subpopulation is larger than the firing rate E_F of the facilitating subpopulation (i.e., say, $E_D = k E_F$, with k > 1). This configuration of firing rates is forced by the external input component, which alternates in time and across the subpopulations. Under these conditions, the STDP would modify intra-population synaptic coupling J_{DD} as follows:

$$\Delta J_{DD} = -A_2^- \tau_{o_1} E_D^2 + A_3^+ \tau_{r_1} \tau_{o_2} E_D^3$$
(S43)

while for the intra-population synaptic couplings, the STDP results into:

Connectivity Motifs by Synaptic Plasticity

$$\Delta J_{DF} = -\frac{1}{k} A_2^- \tau_{o_1} E_D^2 + \frac{1}{k} A_3^+ \tau_{r_1} \tau_{o_2} E_D^3$$
(S44)

$$\Delta J_{FD} = -\frac{1}{k} A_2^- \tau_{o_1} E_D^2 + \frac{1}{k^2} A_3^+ \tau_{r_1} \tau_{o_2} E_D^3$$
(S45)

It is now easy to prove that $\Delta J_{DD} > \Delta J_{DF} > \Delta J_{FD}$, hence identical initial values for J_{DD} , J_{DF} , and J_{FD} would slowly modified heterogeneously and leading to $J_{DD} > J_{DF}$ and to $J_{DD} > J_{FD}$. Similar considerations can be repeated when the firing rate E_F of the facilitating subpopulation is larger than the firing rate E_D of the depressing subpopulation (i.e., say, $E_F = k E_D$, with k > 1), concluding that all in all that the stimulation protocol would shape synaptic efficacies as $J_{DD} > J_{DF}$, $J_{DD} > J_{FD}$, $J_{FF} > J_{DF}$, and $J_{FF} > J_{FD}$, therefore privileging intra-population coupling to inter-population ones, as shown in Fig. S5B.

A.7 Statistics of the symmetry index

In order to quantify and describe concisely the symmetries of the emerging network connectivity matrix $[A_{ij}]$ of size $N \times N$, we defined the following quantity (but see e.g., (45), for alternative definitions):

$$s = 1 - \frac{1}{(0.5 N(N-1) - M)} \sum_{i=1}^{N} \sum_{j=i+1}^{N} |A_{ij}^* - A_{ji}^*|$$
(S46)

s intuitively represents the mean absolute difference between elements that are on symmetric positions, with respect to the diagonal of the matrix. By definition, the elements A_{ij}^* are obtained from A_{ij} upon first normalizing its numerical values to the maximal allowed A_{max} and then clipping them to a lower fraction z. For instance, choosing z = 2/3, if $A_{ij} > 2/3$ A_{max} then $A_{ij}^* = A_{ij} / A_{max}$, and otherwise $A_{ij}^* = 0$. In the Eq. S46, M represents the number of null pairs $\{A_{ij}^*, A_{ji}^*\} = \{0, 0\}$ as a consequence of clipping. Then, s can be rewritten in terms of an arithmetic average of a set of K observations of a random variable q:

$$s = 1 - \frac{1}{K} \sum_{i=1}^{K} q_i$$
 (S47)

Assuming for simplicity that each element of $[A_{ij}]$ is independently drawn from a uniform distribution (i.e., between 0 and A_{max}), the probability density distribution of q, $f_q(Q)$, can be

derived analytically (98). Because the arithmetic average is an unbiased estimator of the expected value of the random variable it samples (i.e., in this case q) (98), most of the statistical properties of s can be immediately derived from the distribution of q. First of all, the expected value of s is given by the expression below

$$\langle s \rangle = A_{max} \left(1 - \frac{1-z}{1-z^2} \left[\frac{(1-z)^2}{3} + z (1+z) \right] \right)$$
 (S48)

Deriving the expression for the variance is less straightforward and requires estimating the expected value of 1/K. In fact K coincides with the number of terms in the double sum of Eq. S46 and it is by definition not a fixed quantity, but a realization of a binomial random variable. An approximated expression for the variance of s is then

$$Var\{s\} \approx A_{max}^2 \frac{2}{N(N-1)(1-z^2)} \left(1 + \frac{2z^2}{N(N-1)(1-z^2)}\right) Var\{q\}$$
 (S49)

where

$$Var\{q\} = \frac{1}{1-z^2} \left(\frac{(1-z)^4}{6} + \frac{2 z (1-z^3)}{3}\right) - (1-\langle s \rangle)^2$$
(S50)

The validity of all the above expressions have been tested and validated numerically, directly estimating the average and variance of s across thousands of uniform random matrices $[A_{ij}]$, for several values of z in the range [0.1;0.9], finding an excellent agreement.

Finally, from the Central Limit Theorem (98), we can expect the density distribution of s to be approximately Gaussian, at least for small values of z. By the above statistical expressions, when studying the impact of short- and long-term synaptic plasticity in shaping microcircuit connectivity motifs (see Figs. 1-2,5), we expressed the significance of the observed values of s as the chance level, i.e., the (Gauss-distributed) probability that the observed value of s could be obtained by chance from a random uniform matrix.

A.8 Alternative STDP models

A.8.1 Pair-based STDP model

By appropriately choosing A_2^+ , A_2^- , and setting to zero both A_3^+ and A_3^- , earlier phenomenological models of pair-based STDP can be rephrased as a special case of the triplet-based model. For the pair-based STDP, each neuron of the network needs only two indicator variables, i.e., q_1 and o_1 , instead of four. In the lack of any firing activity of the *j*-th neuron, those variables exponentially relax to zero:

$$\tau_{q_1} \dot{q}_{1_j} = -q_{1_j} \qquad \tau_{o_1} \dot{o}_{1_j} = -o_{1_j} \tag{S51}$$

As the *j*-th neuron fires, the variables must be instantaneously updated. For such update rule, there are two distinct scenarios determining how successive pre-post or post-pre events interact and affect synaptic efficacy: i) *all-to-all* spike pairs interactions,

$$q_{1_i} \to q_{1_i} + 1 \qquad o_{1_i} \to o_{1_i} + 1 \tag{S52}$$

and ii) nearest-spike interactions,

$$q_{1_j} \to 1 \qquad o_{1_j} \to 1. \tag{S53}$$

where the update rules do not allow accumulation of effects. Finally, when the j-th neuron spikes, the following updates are performed over all the indexes i:

$$\begin{cases} W_{ij} \to W_{ij} - \eta \ A_2^- \ o_{1_i}(t) \\ W_{ji} \to W_{ji} + \eta \ A_2^+ \ q_{1_i}(t) \end{cases}$$
(S54)

Following the considerations by Pfister and Gerstner (54), pair-based models of STDP with all-to-all interactions must be excluded, as they do not reproduce realistic (i.e., BCM) features of synaptic plasticity. We then consider the triplet-based STDP model and alter some of its parameters as it follows: $A_3^+ = A_3^- = 0$, $A_2^+ = 4.5 \ 10^{-3}$, $A_2^- = 7.1 \ 10^{-3}$. We also replaced the *all-to-all* spike pairs interactions by a *nearest spike* interaction, by modifying the update rule for q_1 and r_1 (and for q_2 and r_2 , although those state variables are anyway irrelevant, upon setting $A_3^+ = A_3^- = 0$). By doing so, we obtain the pair-based STDP plasticity rule matching the exact same temporal window of the STDP triplet model employed here. In order to prove that there is correspondence in terms of the temporal window, but altered frequency-dependence, we subjected both the triplet-based and the pair-based models to 75 pairing events, at low frequency 10Hz. The STDP temporal windows at such a frequency are undistinguishable from each other (compare Fig. 2A with Fig. 3A). The frequency-dependence is computed across the same number of pairing events, imposing a pre-post or post-pre delay of 10msec. Note that for sufficiently large frequency of the pre-post pairs, the curves corresponding to pre-post and to post-pre become symmetric with respect to a horizontal line (see Fig. 3B; i.e., around 75 - 80%, corresponding to long-term depression). Such a symmetry implies that in the case of random occurrence of pre-post or post-pre timing, the LTP and the LTD components would cancel each other on the average.

A.8.2 Triplet-based anti-STDP model

This model is obtained from the triplet-based, by setting $A_3^+ = 7.1 \ 10^{-3}$, $A_3^- = 6.1 \ 10^{-3}$, $A_2^+ = 0$, and $A_2^- = 3.5 \ 10^{-3}$, by leaving unchanged the update rules for q_1 , q_2 , o_1 , and o_2 as in the original triplet model, and by modifying the actual weight update equations as it follows: when the *j*-th neuron spikes, the following updates are performed for all the indexes *i*:

$$W_{ij} \to W_{ij} + \eta \ o_{1_i}(t) \left[A_2^+ + A_3^+ \ q_{2_j}(t-\epsilon) \right]$$

$$W_{ji} \to W_{ji} - \eta \ q_{1_i}(t) \left[A_2^- + A_3^- \ o_{2_j}(t-\epsilon) \right]$$
(S55)

Note that this is only a tentative proposal for an anti-STDP rule, since experimental of data is not yet available for all induction protocols earlier employed for STDP. In particular, we ignore the frequency-dependency of the anti-STDP and by the new parameter set we roughly leave it untouched (compare Fig. 2B with Fig. 3D).

References

- Seung H (2009) Reading the book of memory: Sparse sampling reading the book of memory: Sparse sampling versus dense mapping of connectomes. Neuron 62: 17-29.
- 2. Wickersham I, Lyon E DC Barnard, Mori T, Finke S, Conzelmann K, et al. (2007) Monosynaptic restriction of transsynaptic tracing from single, genetically targeted neurons. Neuron

53: 639-47.

- 3. Zhang F, Aravanis A, Adamantidis A, de Lecea L, Deisseroth K (2007) Circuit-breakers: optical technologies for probing neural signals and systems. Nat Rev Neurosci 8: 577-81.
- Lichtman J, Livet J, Sanes J (2008) A technicolour approach to the connectome. Nat Rev Neurosci 9: 417-22.
- 5. Denk W, Horstmann H (2004) Serial block-face scanning electron microscopy to reconstruct three-dimensional tissue nanostructure. PLoS Biol 2: e329.
- Chklovskii D, Vitaladevuni S, Scheffer L (2010) Semi-automated reconstruction of neural circuits using electron microscopy. Current Opinion in Neurobiology 20: 667–75.
- Song S, Sjöström P, Reigl M, Nelson S, Chklovskii D (2005) Highly nonrandom features of synaptic connectivity in local cortical circuits. PLoS Biol 3: e68.
- Hai A, Shappir J, Spira M (2010) In-cell recordings by extracellular microelectrodes. Nat Methods 7: 200-2.
- Perin R, Berger T, Markram H (2011) A synaptic organizing principle for cortical neuronal groups. Proc Nat Acad Sci USA 108: 5419-24.
- Friston K (2011) Functional and effective connectivity: A review. Brain Connectivity 1: 13-36.
- Minderer M, Liu W, Sumanovski L, Kügler S, Helmchen F, et al. (2012) Chronic imaging of cortical sensory map dynamics using a genetically encoded calcium indicator. J Physiol 590: 99-107.
- 12. Wedeen V, Rosene D, Wang R, Dai G, Mortazavi F, et al. (2012) The geometric structure of the brain fiber pathways. Science 335: 1628-34.
- 13. Kandell E, Schwartz J, Jessel A (2008) Principles of Neural Science. McGraw-Hill.
- Silberberg G, Grillner S, LeBeau F, Maex R, Markram H (2005) Synaptic pathways in neural microcircuits. Trends in Neuroscience 28: 541-51.
- Grillner S, Markram H, De Schutter E, Silberberg G, LeBeau F (2005) Microcircuits in action - from cpgs to neocortex. Trends in Neuroscience 28: 525-33.

- Douglas R, Martin K (2007) Recurrent neuronal circuits in the neocortex. Curr Biology 17: R496-500.
- 17. Douglas R, Martin K (2007) Mapping the matrix: the ways of neocortex. Neuron 56: 226-38.
- Binzegger T, Douglas K RJ Martin (2004) A quantitative map of the circuit of cat primary visual cortex. J Neurosci 24: 8441-53.
- Wang Y, Markram H, Goodman P, Berger T, Ma J, et al. (2006) Heterogeneity in the pyramidal network of the medial prefrontal cortex. Nat Neurosci 9: 534-42.
- Silberberg G, Markram H (2007) Disynaptic inhibition between neocortical pyramidal cells mediated by martinotti cells. Neuron 53: 735-46.
- 21. Tsodyks M, Markram H (1997) The neural code between neocortical pyramidal neurons depends on neurotransmitter release probability. Proc Nat Acad Sci USA 94: 719-23.
- 22. Varela J, Sen K, Gibson J, Fost J, Abbott L, et al. (1997) A quantitative description of short-term plasticity at excitatory synapses in layer 2/3 of rat primary visual cortex. J Neurosci 17: 7926-40.
- Buonomano DV, Merzenich M (1998) Cortical plasticity: From synapses to maps. Annu Rev Neurosci 21: 149-86.
- Markram H, Gerstner W, Sjöström P (2011) A history of spike-timing-dependent plasticity. Front Synaptic Neurosci 3: 1-24.
- Chklovskii D, Mel B, Svoboda K (2004) Cortical rewiring and information storage. Nature 431: 782-8.
- Le Be' V, Markram H (2006) Spontaneous and evoked synaptic rewiring in the neonatal neocortex. P Natl Acad Sci USA 103: 13214-9.
- Haeusler S, Schuch K, Maass W (2009) Motif distribution, dynamical properties, and computational performance of two data-based cortical microcircuit templates. J Physiol (Paris) 103: 73-87.
- 28. Cowan W, Sudhof T, Stevens C (2003) Synapses. The Johns Hopkins Univ. Press.

- Pignatelli M (2009) Structure and Function of the Olfactory Bulb Microcircuit. Ph.D. thesis,
 École Polytechnique Fédérale de Lausanne, http://library.epfl.ch/en/theses/?nr=4275.
- Clopath C, Buesing L, Vasilaki E, Gerstner W (2010) Connectivity reflects coding: a model of voltage-based stdp with homeostasis. Nat Neurosci 13: 344-52.
- Tsodyks M, Pawelzik K, Markram H (1998) Neural networks with dynamic synapses. Neural Comp 10: 821-35.
- Brette R, Gerstner W (2005) Adaptive exponential integrate-and-fire model as an effective description of neuronal activity. J Neurophysiol 94: 3637-42.
- Tsodyks M (2005) Methods and models in neurophysics, Elsevier, chapter Synaptic Dynamics. pp. 245-66.
- 34. Renart A, Brunel N, Wang X (2004) Mean-Field Theory of Irregularly Spiking Neuronal Populations and Working Memory in Recurrent Cortical Networks, volume Computational Neuroscience: A Comprehensive Approach. CRC Press.
- Pfister JP, Gerstner W (2006) Triplets of spikes in a model of spike timing-dependent plasticity. J Neurosci 26: 9673-82.
- Barak O, Tsodyks M (2007) Persistent activity in neural networks with dynamic synapses.
 PLoS Comput Biol 3: e35.
- 37. Gjorgjieva J, Clopath C, Audet A, Pfister JP (2011) A triplet spike-timing-dependent plasticity model generalizes the bienenstock-cooper-munro rule to higher-order spatiotemporal correlations. Proc Nat Acad Sci USA 108: 19383–8.
- Sjöström P, Turrigiano G, Nelson S (2001) Rate, timing, and cooperativity jointly determine cortical synaptic plasticity. Neuron 32: 1149-1164.
- Liu Y, Wang X (2001) Spike-frequency adaptation of a generalized leaky integrate-and-fire model neuron. J Comput Neurosci 10: 25-45.
- 40. Brunel N, Amit D (1997) Model of global spontaneous activity and local structured activity during delay periods in the cerebral cortex. Cereb Cortex 7: 237-52.

- Roxin A, Brunel N, Hansel D, Mongillo G, Van Vreeswijk C (2011) On the distribution of firing rates in networks of cortical neurons. J Neurosci 31: 16217-26.
- Tuckwell H (1989) Stochastic Processes in the Neurosciences. Society for Industrial and Applied Mathematics.
- Sterrat D, Graham B, Gillies A, Willshaw D (2011) Principles of Computational Modelling in Neuroscience. Cambridge University Press.
- Morrison A, Diesmann M, Gerstner W (2008) Phenomenological models of synaptic plasticity based on spike timing. Biological Cybernetics 98: 459-78.
- 45. Huber L, Baker F (1979) Evaluating the symmetry of a proximity matrix. Quality and Quantity 13: 77-84.
- Wilson H, Cowan J (1972) Excitatory and inhibitory interactions in localized populations of model neurons. Biophys J 12: 1-24.
- Dayan P, Abbott L (2001) Theoretical neuroscience: computational and mathematical modeling of neural systems. The MIT Press: Cambridge, Massachusetts.
- 48. La Camera G, Giugliano M, Senn W, Fusi S (2008) The response of cortical neurons to in vivo-like input current: theory and experiment i. noisy inputs with stationary statistics. Biological Cybernetics 99: 279-301.
- 49. Giugliano M, La Camera G, Fusi S, Senn W (2008) The response of cortical neurons to in vivo-like input current: theory and experiment ii. time-varying and spatially distributed inputs. Biological Cybernetics 99: 303-18.
- Markram H, Tsodyks M (1996) Redistribution of synaptic efficacy between neocortical pyramidal neurones. Nature 382: 807-9.
- 51. Abbott L, Nelson S (2000) Synaptic plasticity: taming the beast. Nat Neurosci 3: 1178-83.
- Song S, Miller K, Abbott L (2000) Competitive hebbian learning through spike-timingdependent synaptic plasticity. Nat Neurosci 3: 919-26.
- Rubin J, Lee D, Sompolinsky H (2001) Equilibrium properties of temporally asymmetric hebbian plasticity. Phys Rev Lett 86: 364-7.

- 54. Pfister JP, Gerstner W (2006) Beyond pair-based stdp: A phenomenological rule for spike triplet and frequency effects. MIT Press, volume 17 of Advances in Neural Inf. Proc. Syst., pp. 1409-16.
- 55. Bi G, Rubin J (2005) Timing in synaptic plasticity: from detection to integration. Trends in Neuroscience 28: 222-8.
- Holcman D, Tsodyks M (2006) The emergence of up and down states in cortical networks. PLoS Comput Biol 2: e23.
- 57. Del Giudice P, Fusi S, Mattia M (2003) Modelling the formation of working memory with networks of integrate-and-fire neurons connected by plastic synapses. J Physiol (Paris) 97: 659-681.
- Del Giudice P, Mattia M (2001) Long and short-term synaptic plasticity and the formation of working memory: A case study. Neurocomputing 38-40: 1175-1180.
- 59. Strogatz S (1994) Nonlinear dynamics and chaos. Reading, MA (USA): Addison Wesley.
- 60. Kempter R, Gerstner W, Van Hemmen J, Wagner H (1996) Temporal coding in the submillisecond range: model of barn owl auditory pathway. Advances in neural information processing systems : 124–130.
- Gerstner W, Kempter R, Van Hemmen J, Wagner H (1996) A neuronal learning rule for sub-millisecond temporal coding. Nature 383: 76–78.
- 62. Bower J, Haberly L (1986) Facilitating and nonfacilitating synapses on pyramidal cells: a correlation between physiology and morphology. Proc Nat Acad Sci USA 83: 1115-9.
- Stratford K, Tarczy-Hornoch K, Martin K, Bannister N, Jack J (1996) Excitatory synaptic inputs to spiny stellate cells in cat visual cortex. Nature 382: 258-61.
- 64. Reyes A, Sakmann B (1999) Developmental switch in the short-term modification of unitary epsps evoked in layer 2/3 and layer 5 pyramidal neurons of rat neocortex. J Neurosci 19: 3827-35.
- Geracitano R, Kaufmann W, Szabo G, Ferraguti F, Capogna M (2007) Synaptic heterogeneity between mouse paracapsular intercalated neurons of the amygdala. J Physiol 585: 117-34.

- Markram H, Wang Y, Tsodyks M (1998) Differential signaling via the same axon of neocortical pyramidal neurons. Proc Nat Acad Sci USA 95.
- Morrison A, Aerstsen A, Diesmann M (2007) Spike-timing-dependent plasticity in balanced random networks. Neural Comp 19: 1437-67.
- Gilson M, Burkitt A, van Hemmen J (2010) Stdp in recurrent neuronal networks. Front Comput Neurosci 4: 1-15.
- 69. Gilson M, Burkitt A, Grayden D, Thomas D, van Hemmen J (2009) Emergence of network structure due to spike-timing-dependent plasticity in recurrent neuronal networks. iii: Partially connected neurons driven by spontaneous activity. Biological Cybernetics 101: 411-26.
- 70. Kunkel S, Diesmann M, Morrison A (2011) Limits to the development of feed-forward structures in large recurrent neuronal networks. Front Comput Neurosci 4.
- Bourjaily M, Miller P (2011) Excitatory, inhibitory, and structural plasticity produce correlated connectivity in random networks trained to solve paired-stimulus tasks. Front Comput Neurosci 5: 1-24.
- 72. Song S, Abbott L (2001) Column and map development and cortical re-mapping through spike-timing dependent plasticity. Neuron 32: 339-50.
- Butts D, Kanold P (2010) The applicability of spike time dependent plasticity to development. Front Synaptic Neurosci 2: 1-9.
- Cooper L, Intrator N, Blais B, Shouval H (2004) Theory of Cortical Plasticity. World Scientific, Singapore.
- 75. Fuhrmann G, Segev I, Markram H, Tsodyks M (2002) Coding of temporal information by activity-dependent synapses. J Neurophysiol 87: 140-8.
- 76. Fuhrmann G, Cowan A, Segev I, Tsodyks M, Stricker C (2004) Multiple mechanisms govern the dynamics of depression at neocortical synapses of young rats. J Physiol 557: 415-38.
- 77. Loebel A, Silberberg G, Helbig D, Markram H, Tsodyks M, et al. (2009) Multiquantal release underlies the distribution of synaptic efficacies in the neocortex. Front Comput Neurosci 3.

- Pan B, Zucker R (2009) A general model of synaptic transmission and short-term plasticity. Neuron 62: 539-54.
- Rubin J, Gerkin R, Bi G, Chow C (2005) Calcium time course as a signal for spike-timingdependent plasticity. J Neurophysiol 93: 2600-13.
- Graupner M, Brunel N (2012) Calcium-based plasticity model explains sensitivity of synaptic changes to spike pattern, rate, and dendritic location. Proc Nat Acad Sci USA 109: 3991-6.
- Vogels T, Rajan K, Abbott L (2005) Neural network dynamics. Annu Rev Neurosci 28: 357-76.
- Gigante G, Del Giudice P, Mattia M (2007) Frequency-dependent response properties of adapting spiking neurons. Mathematical Biosciences 2: 336-51.
- 83. Rauch A, La Camera G, Luescher H, Senn W, Fusi S (2003) Neocortical pyramidal cells respond as integrate-and-fire neurons to in vivo-like input currents. J Neurophysiol 90: 1598-612.
- Pimentel D, Margrie T (2008) Glutamatergic transmission and plasticity between olfactory bulb mitral cells. J Physiol 586.8: 2107-119.
- Cassenaer S, Laurent G (2012) Conditional modulation of spike-timing dependent plasticity for olfactory learning. Nature doi:10.1038/nature10776.
- Gao Y, Strowbridge B (2009) Long-term plasticity of excitatory inputs to granule cells in the rat olfactory bulb. Nat Neurosci 12: 731-3.
- 87. Linster C, Cleland T (2010) Decorrelation of odor representations via spike timing-dependent plasticity. Front Comput Neurosci 4: 1-11.
- Buonomano DV (1999) Distinct functional types of associative long-term potentiation in neocortical and hippocampal pyramidal neurons. J Neurosci 19: 6748-54.
- Markram H, Pikus D, Gupta A, Tsodyks M (1998) Potential for multiple mechanisms, phenomena and algorithms for synaptic plasticity at single synapses. Neuropharmacology 37: 489-500.

- Mongillo G, Barak O, Tsodyks M (2008) Synaptic theory of working memory. Science 319: 1543-6.
- 91. Bi G, Poo M (1998) Synaptic modifications in cultured hippocampal neurons: dependence on spike timing, synaptic strength, and postsynaptic cell type. J Neurosci 18: 10464–72.
- 92. Barabasi A (2005) Taming complexity. Nature Physics 1: 68-70.
- Froemke R, Dan Y (2002) Spike-timing-dependent synaptic modification induced by natural spike trains. Nature 416: 433-438.
- 94. Clopath C, Gerstner W (2010) Voltage and spike timing interact in stdp a unified model. Front Synaptic Neurosci 2.
- 95. Kepecs A, van Rossum MC, Song S, Tegner J (2002) Spike-timing-dependent plasticity: common themes and divergent vistas. Biological Cybernetics 87: 446-58.
- 96. Mattia M, Del Giudice P (2004) Finite-size dynamics of inhibitory and excitatory interacting spiking neurons. Phys Rev E Stat Nonlin Soft Matter Phys 70: 052903.
- 97. Press W, Teukolsky S, Vetterling W, Flannery B (2007) Numerical Recipes: The Art of Scientific Computing. Cambridge University Press.
- 98. Papoulis A, Pillail SU (2002) Probability, random variables, and stochastic processes. McGraw-Hill, 4th edition.

Figures and Figure Legends

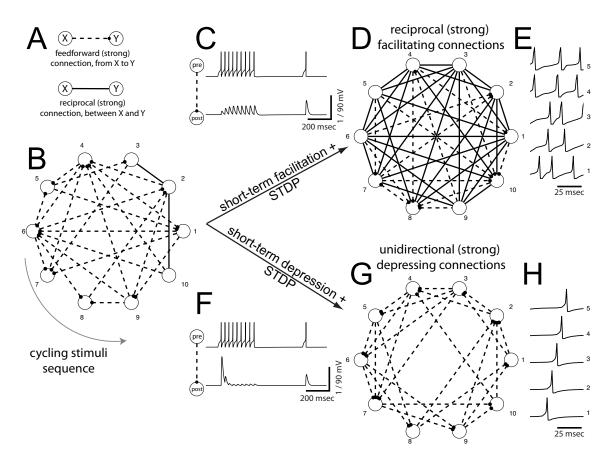


Figure 1. Emergence of connectivity motifs in a toy model network. Unidirectional (reciprocal) strong excitatory connections are indicated (A) as dashed (continuous) line segments, representing the topology of the network (B). Each model neuron receives periodic spatially alternating depolarizing current pulses, strong enough to make it fire a single action potential. Synapses among connected neurons display (C) short-term facilitation of postsynaptic potential amplitudes. Spike-Timing Dependent Plasticity (STDP) leads to strengthened connections and result into a largely reciprocal topology (D). Modifying the short-term plasticity profile into depressing (F), leads to a largely unidirectional topology shaped by STDP(G). Distinct motifs of strong connections arise from short- and long-term plasticities, due to distinct firing patterns (compare E and H), under identical external stimulation and initial connections. Parameters: $A_{ij} = 400pA$.

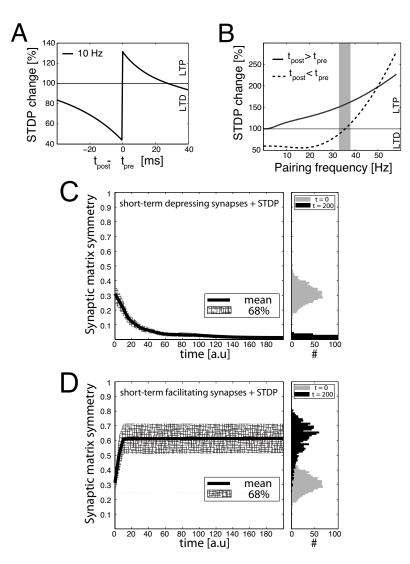


Figure 2. Statistics of motifs emergence in a toy model network. When decoupled from recurrent interactions, an isolated model synapse undergoes long-term changes depending on preand postsynaptic spike timing (A) and pairing frequency (B). Above a *critical* frequency (gray shading), spike timing no longer matters and long-term potentiation of synaptic efficacy (LTP) prevails on long-term depression (LTD). Panels C, D: The simulations of Fig. 1 were repeated 2000 times, each time starting from a random initial topology. STDP progressively induced a persisting non-random reconfiguration of strong connections, quantified across time by a symmetry index (see Methods). Neurons connected only by short-term depressing synapses evolved strong unidirectional connections, corresponding to a low symmetry index. This is displayed in panel C, as an average across the 2000 simulations (left panel). Initial and final distributions of symmetry index values are also shown (right panel, gray and black histogram respectively). Neurons connected only by short-term facilitating synapses evolved instead strong bidirectional connections with high symmetry indexs (D).

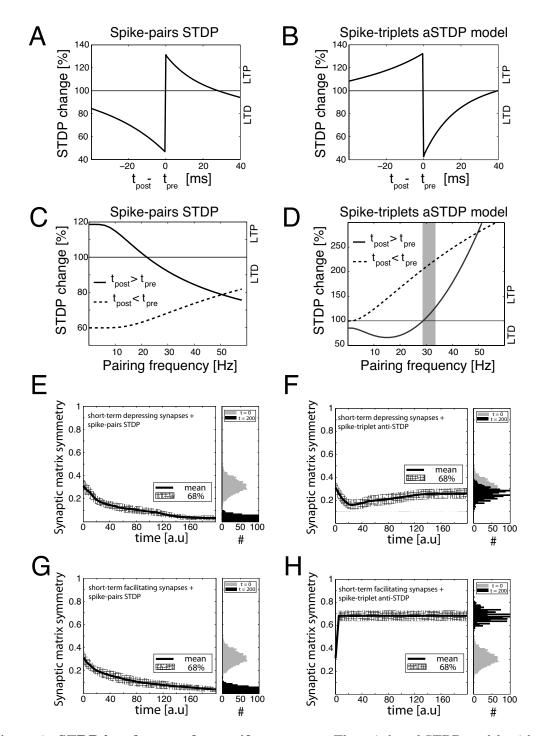


Figure 3. STDP key-features for motif emergence. The pair-based STDP model, with temporal window shown in panel **A** and matching exactly Fig. 2A, exhibits a different frequency-dependency (panel **C**) than the triplet-based STDP model (Fig. 2B). Modifying the triplet-based STDP parameters to ad-hoc invert its temporal window (e.g., as in anti-STDP, panel **B**, compare to panel **A**), yet leaves its frequency-dependency and the LTD-reversal (gray shading) unchanged (panel **D**). Repeating the study of Fig. 2 with these two modified models, we find that i) the pair-based STDP fails to account for motifs emergence (panels **E**,**G**, compare to Fig. 2), while anti-STDP succeeds (panels **F**,**H**, compare to Fig. 2). Parameters: see the Supplemental Information.

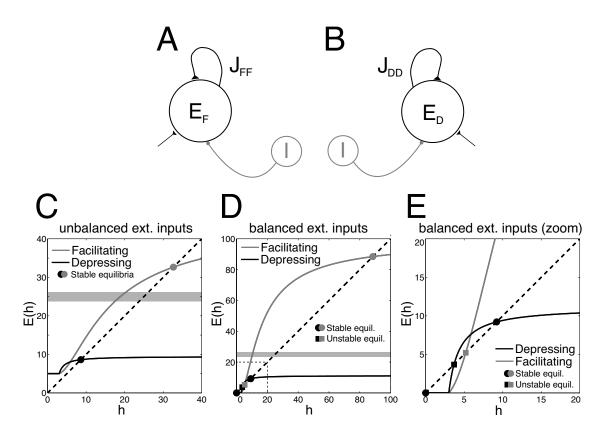


Figure 4. Mean-field analysis of firing rate equilibria, in homogeneous networks without long-term plasticity. The firing rate of homogeneous recurrent networks, including short-term facilitating synapses (A) or depressing excitatory synapses (B), was studied by standard mean-field analysis. Average synaptic efficacies are indicated by J_{FF} or by J_{DD} , correspondingly. Excitatory and inhibitory external inputs are modeled by a single term, taking positive, zero or negative values. A zero value corresponds to *balanced* excitatory/inhibitory inputs, while a non-zero value corresponds to *unbalanced* excitatory/inhibitory inputs. The steady-state firing rate (i.e., E, in a.u.) are the roots of the equation E(h) = h (see Eqs. 10,11 and the Supplemental Information), whose graphical solution is provided (C-E), for facilitating (gray) or depressing (black) synapses, without long-term plasticity. Panel E is a zoomed view of D. (Un)stable firing rate equilibria are indicated by filled circles (squares). Networks with facilitating synapses fire at higher rates than networks with depressing synapses, as emphasized by the gray shading.

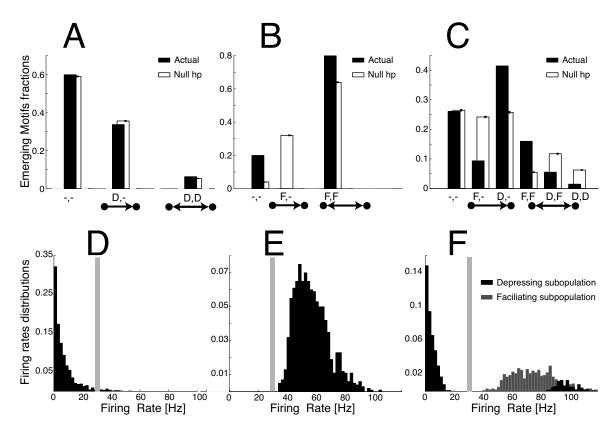


Figure 5. Results from numerical simulations of large recurrent networks of model neurons with short- and long-term plasticity. Homogeneous and heterogeneous recurrent networks made of 1000 Integrate-and-Fire model neurons were numerically simulated, under identical conditions. Panel A shows the comparison of the emergence of weak or no connectivity pairs (indicated as "-,-"), of unidirectional strong connectivity pairs (" \rightarrow ", "D,-"), and of reciprocal strong connectivity pairs (" \leftrightarrow ", "D,D") for a homogeneous network of neurons connected by depressing synapses: strong unidirectional depressing connections significantly outnumber reciprocal depressing ones. The fractions of emerged motifs (black) is significantly different than the null-hypothesis (white) of random motifs occurrence. Panel B repeats this quantification for a homogeneous network with facilitating synapses: strong connections are only found on reciprocal connectivity pairs (" \leftrightarrow ", "F,F") and all emerging motifs are non-random. Panel C repeats the same quantification for a heterogeneous network with both short-term facilitating and depressing synapses. Emerging motifs display highly non-random features and confirm that reciprocal facilitatory motifs (" \leftrightarrow ", "F,F") outnumber unidirectional facilitatory motifs $("\rightarrow", "F,-")$, and that unidirectional depressing motifs $("\rightarrow", "D,-")$ outnumber reciprocal depressing motifs (" \leftrightarrow ", "D,D"). Panels **D-F** display the steady-state firing rate distributions, corresponding to homogeneous depressing, homogeneous facilitating, and heterogeneous networks respectively. The plots confirm that heterogeneity in connectivity motifs is accompanied by bimodal firing rates above and below the *critical* frequency, represented here by a grey shading.

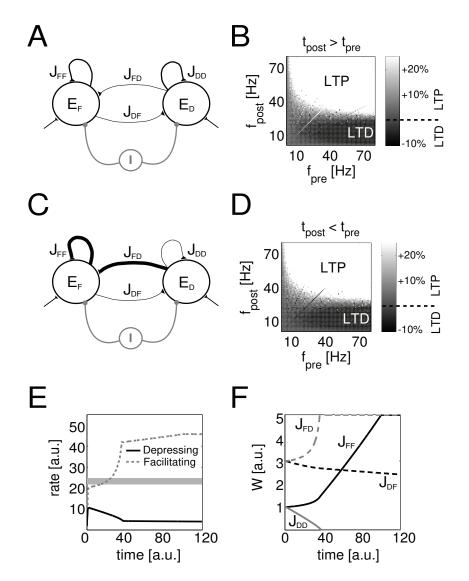


Figure 6. Mean-field simulation of a heterogeneous network with short- and long-term plasticity. The firing rate evolution of a heterogenous recurrent network, including both short-term facilitating and depressing synapses (A), was estimated by numerically solving the corresponding mean-field equations. The average synaptic efficacies among and across populations, indicated by J_{FF} , J_{DD} , J_{FD} , and J_{DF} , undergo long-term modification. Panels **B,D** show the long-term changes of an isolated synapse (decoupled from recurrent interactions) depending on pre- and postsynaptic spike timing (i.e., t_{pre} , t_{post}) and frequencies (i.e., f_{pre} , f_{post}). When f_{pre} and f_{post} are varied independently, long-term potentiation (LTP) and depression (LTD) emerges as in associative Hebbian plasticity. This suggests that J_{FF} and J_{FD} will become significantly stronger than J_{FD} and J_{DD} (C) and that such a configuration will be retained indefinitely. This was confirmed by simulations (**E-F**) plotting the temporal evolution of the firing rates E_F (black trace) and E_D (gray trace), and of the synaptic efficacies (**F**). The heterogeneity occurs by separation of emerging firing rates (Fig. 4), as emphasized by the grey shading. Parameters: $I_{ext} = 5$, $\tau = 10$ msec, with initial conditions $J_{FF} = J_{DD} = 3$, and $J_{DF} = J_{FD} = 1$ (see Supplemental Information for alternatives).

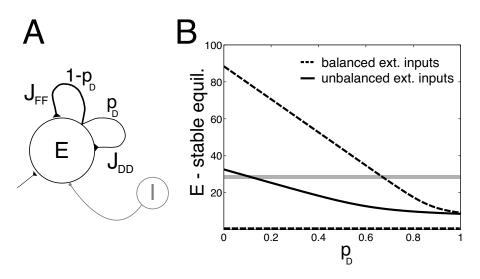


Figure 7. Mean-field analysis of firing rate equilibria, in homogeneous networks with overlapping short-term synaptic properties and no long-term plasticity. Panel A represents the sketch of a recurrent network where a clear segregation between subpopulations of depressing- or facilitating-only synapses does not occur. A neuron has a probability p_D of connecting to its postsynaptic target by a depressing synapse, and $1 - p_D$ of connecting to its target by a facilitating synapse. Panel B plots the location of the equilibria of the firing rate E, under distinct external inputs conditions and for increasing values of p_D . For the same parameters of Fig. 4, stable equilibria move as a function of p_D , taking intermediate values between the two extreme cases, i.e., $p_D = 0$ and $p_D = 1$; compare to panels D-F of Figs. 4.

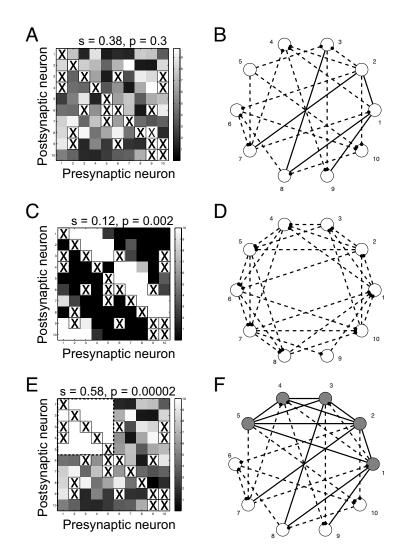


Figure 8. External activity may still induce reciprocal motifs emergence in depressing networks. As in Figure 1, the synaptic connectivity matrix of a network of ten neurons was randomly initialized and pruned (\mathbf{A}, \mathbf{B} , i.e., pruning is indicated by the "X" symbols). Internally generated activity, as in Figures 1-2, contributes to the emergence of non-random unidirectional motifs, resulting in an asymmetric matrix W (\mathbf{C}, \mathbf{D}). However, if five units of the same network (gray circles) are externally stimulated above the STDP *critical* frequency (see the Results of the main text), a non-random connectivity emerges, featuring reciprocal motifs and a symmetric connectivity submatrix (\mathbf{E}, \mathbf{F} ; upper left corner, dashed rectangle). The values indicated above panels $\mathbf{A}, \mathbf{C}, \mathbf{E}$ represent the symmetry index and its significance.

Symbol	Description	Value
dt	Forward Euler method integration time step	$0.1\ msec$
N	Number of simulated neurons	10 - 1000
c_m	Membrane capacitance	$281 \ pF$
g_{leak}	Membrane leak conductance	$30 \ nS$
E_{leak}	Resting membrane potential	-70.6 mV
E_{reset}	After-spike reset potential	-70.6 mV
Δ_T	Spike steepness of the exponential IF model	2 mV
V_{θ}	Spike emission threshold of the exponential IF model	20 mV
V_T	Threshold voltage parameter of the exponential IF model	-50.4 mV
$ au_{arp}$	Absolute refractory period	2 msec
a	Voltage dependence coefficient of the spike frequency adaptation	4 nS
Δ_x	Spike-timing dependence parameter of the spike frequency adaptation	$0.0805 \ nA$
$ au_x$	Time constant of the spike frequency adaptation	$144\ msec$
$ au_{syn}$	Excitatory postsynaptic currents decay time constant	5 msec
U_D	Release probability, for depressing synapses	0.8
U_F	Release probability, for facilitatory synapses	0.1
$\tau_{rec D}$	Time constant of recovery from depression, for <i>depressing</i> synapses	$900\ msec$
$ au_{rec}$ F	Time constant of recovery from depression, for <i>facilitating</i> synapses	$100\ msec$
$\tau_{facil} D$	Time constant of recovery from facilitation, for <i>depressing</i> synapses	$100\ msec$
$\tau_{facil} F$	Time constant of recovery from facilitation, for $facilitating$ synapses	$900\ msec$
A_2^-	STDP model LTD amplitude for post-pre event	$7.1 \ 10^{-3}$
A_{3}^{-}	STDP model LTD amplitude for post-pre event (triplet-term)	0
A_2^+	STDP model LTP amplitude for pre-post event	0
A_{3}^{+}	STDP model LTP amplitude for pre-post event (triplet-term)	$6.5 \ 10^{-3}$
$ au_{q_1}$	STDP model decay time of presynaptic indicator q_1	$16.8\ msec$
$ au_{q_2}$	STDP model decay time of presynaptic indicator q_2	$101\ msec$
$ au_{o_1}$	STDP model decay time of postsynaptic indicator o_1	$33.7 \ msec$
$ au_{o_2}$	STDP model decay time of postsynaptic indicator o_2	$114\ msec$
$A_{i \ j}$	Maximal synaptic efficacy	$6 - 12 \ pA$
W_{max}	Upper boundary for STDP dimensionless scaling factor W_{ij}	5
θ	Threshold of the frequency-current response curve for mean-field models	3
η	STDP plasticity rate	1

Table 1. Parameters employed in the simulations: STDP parameters are as in the *minimal all-to-all* triplet model described in Pfister and Gerstner (2006); short-term depression and facilitation parameters as in (Wang *et al.*, 2006); neuron parameters are as in (Clopath *et al.*, 2010).

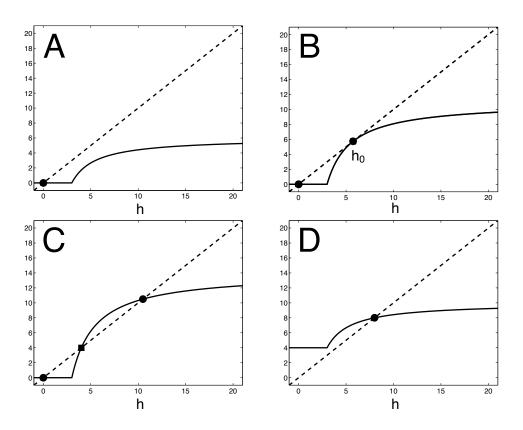


Figure S1. Graphical representation of the function $F_2(h)$, for different values of A and I_{ext} . The function $F_2(h)$ has been plotted for different values of the maximal synaptic efficacy A and external input I_{ext} , resulting in one intersection only ($\mathbf{A} - A = 3$, $I_{ext} = 0$), three intersections with two of them coincident with each other ($\mathbf{B} - A = 5.488$, $I_{ext} = 0$), three distinct intersections ($\mathbf{C} - A = 7$, $I_{ext} = 0$), and finally one intersection for larger external input ($\mathbf{D} - A = 3$, $I_{ext} = 4$). The remaining parameters were: U = 0.8, $\tau_{rec} = 500 \text{ msec}$, $\theta = 3$, $\alpha = 1$. The scripts to generate these plots and to carry out asymptotic analysis on the stability of the equilibrium points, see the text, are available online from the ModelDB (accession number 143082).

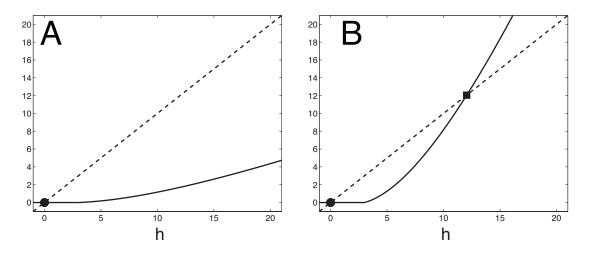


Figure S2. Graphical representation of the function $F_3(h)$, for different values of A. The function $F_3(h)$ has been plotted for different values of the maximal synaptic efficacy A and external input I_{ext} , resulting in one (A - A = 0.5, $I_{ext} = 0$) or two intersections (B - A = 3.5, $I_{ext} = 0$). The remaining parameters were: U = 0.1, $\tau_{facil} = 500 \text{ msec}$, $\theta = 3$, $\alpha = 1$. The scripts to generate these plots and to carry out asymptotic analysis on the stability of the equilibrium points, see the text, are available online at the ModelDB (accession number 143082).

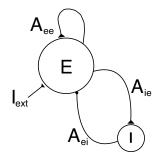


Figure S3. Mean field description for two recurrently connected populations of excitatory and inhibitory neurons. Excitatory neurons are recurrently connected by short-term plastic synapses and project to a population of inhibitory neurons. Inhibitory neurons project back to the excitatory population with non-plastic, linear synapses.

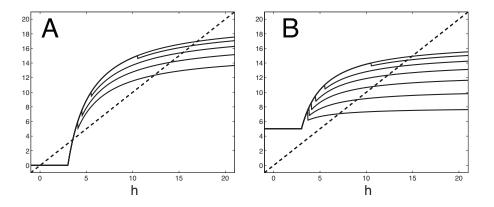


Figure S4. Graphical representation of the equivalent of functions $F_2(h)$ and $F_3(h)$, in the presence of inhibition. Increasing the coupling between the excitatory and the inhibitory population substantially bends down the curves previously analyzed as $F_2(h)$ and $F_4(h)$, lowering the firing rate of the equilibrium points ($A_{ei} = A_{ie} / 10$; $\mathbf{A} - I_{ext} = 0$, $\mathbf{B} - I_{ext} = 5$).

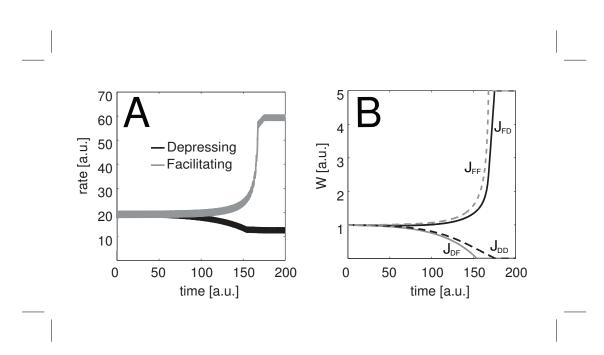


Figure S5. Formation of asymmetric intra and extra population synapses. The subopulations D and F of Fig. 4A receive a common input current ($I_C = 12.5$) and an alternating stimulation component (I_{ED} , I_{EF}), oscillating periodically between two amplitude levels (i.e., 2 and 0) every 1 [a.u.] of time: whenever $I_{ED} = 0$, $I_{EF} = 2$, and vice versa. The temporal evolution of the firing rate of each population is shown in **A**, while the corresponding long-lasting plastic changes of the synaptic coupling (i.e., J_{FF} , J_{DD} , J_{FD} , J_{DF}) is plotted in **B**, upon initialization to the same value (i.e., 1). The same final configuration is generally obtained even by randomly initializing J_{FF} , J_{DD} , J_{FD} , and J_{DF} by a Gaussian distribution with mean 1 and standard deviation 0.001, for 90 out of 100 simulation runs, demonstrating a degree of robustness.

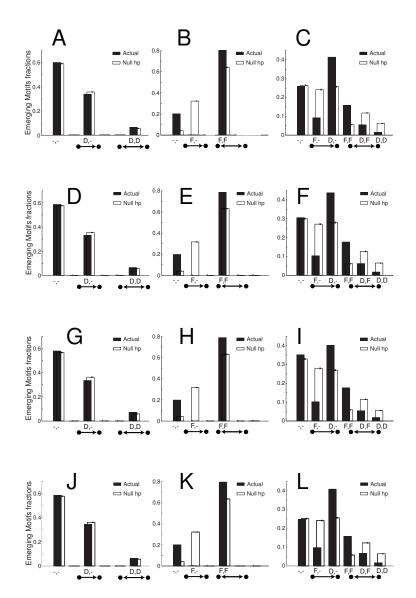


Figure S6. External stimulation protocols and models details do not affect motifs emergence. The figure examines the fraction of motifs, emerging when neurons receive periodic input wave-like stimulation ($\mathbf{A}, \mathbf{B}, \mathbf{C}$, exactly as in Figure 6A-C, for ease of comparison). However, when the periodic stimulation is omitted ($\mathbf{D}, \mathbf{E}, \mathbf{F}$), as well as when each neuron receives instead a ten percent shared random background inputs with each other ($\mathbf{G}, \mathbf{H}, \mathbf{I}$), very similar results emerge. The simulations of panels $\mathbf{D}, \mathbf{E}, \mathbf{F}$, when repeated without spike-frequency adaptation mechanisms from each unit of the network(s) ($\mathbf{J}, \mathbf{K}, \mathbf{L}$), still give rise to the same results.

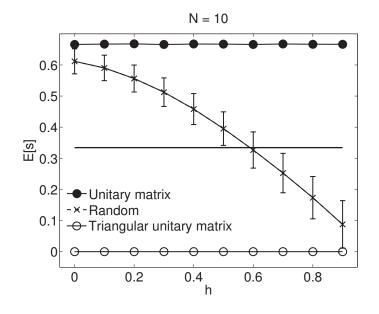


Figure S7. Impact of the clipping threshold parameter h on the symmetry measure s. The continuous trace and \times markers show the expectation of the symmetry index for a random connectivity matrix with 20% of its elements randomly pruned, over 10000 samples of 10×10 matrices, with error bars indicating the standard deviation. The simulations were repeated for a unitary matrix (i.e., leading to the maximum possible value for s) and for a upper triangular unitary matrix (i.e., leading to the minimum possible value for s). The value of h = 2/3 used in this work, chosen for consistence to earlier works, leads to a middle point between the two extremes considered and thus provide a good discriminating condition when using the statistics of a random matrix as a null hypothesis.